DISCHARGE CHARACTERISTICS OF A
CARBON DIOXIDE TEA LASER

Ronald Floyd Bishop

NAVAL POSTGRADUATE SCHOOL
Monterey, California

THESIS

DISCHARGE CHARACTERISTICS

OF A

CARBON DIOXIDE TEA LASER

by

Ronald Floyd Bishop

Thesis Advisor: N. M. Ceglio

December 1972

T152952

Discharge Characteristics

of a

Carbon Dioxide TEA Laser

by

Ronald Floyd Bishop
Lieutenant, United States Navy
B.S., United States Naval Academy, 1965

Submitted in partial fulfillment of the
requirements for the degree of

MASTER OF SCIENCE IN PHYSICS

from the

NAVAL POSTGRADUATE SCHOOL
December 1972

ABSTRACT

During the past two years a rapid development in the
field of high pressure CO_2 lasers has been witnessed. How-
ever, in the haste of this development very little effort
had been expended to understand the detailed aspects of the
discharge characteristics of such lasers. The results of a
parametric study of the discharge characteristics of an
atmospheric pressure, double-discharge CO_2 laser are reported.
The results discussed include: A clarification of the impor-
tant role played by helium in establishing good discharge
conditions; measurements of plasma resistivity as a function
of gas content and circuitry elements; establishment of a
satisfactory operating regime in parameter space for a
double-discharge laser with a two centimeter gap; and a dis-
cussion of the major problems limiting the operation of such
a laser. The results presented should be applicable to a
wide class of double-discharge gas lasers.

TABLE OF CONTENTS

LIST OF TABLES

I. <u>INTRODUCTION</u>

In the effort to continue the study of absorption by a laser produced plasma at the Naval Postgraduate School, a carbon dioxide (CO_2) Transverse Excitation at Atmospheric pressure (TEA) laser was constructed. A CO_2 TEA laser is a source of high powered, pulsed, coherent radiation with a wavelength of approximately 10.6 microns. Longer wavelengths are better for heating plasmas with densities on the order of 10^{15} to 10^{19} electrons per cubic centimeter.

The second phase in the process of constructing the TEA laser was the modification of the original designs and physical arrangement of the associated components of the laser system. These changes were necessary to improve the gas flow system, energy transport from the Tachisto Marx generator to the laser electrodes, the end plate portals which contained the NaCl windows, the resonant cavity mirrors and associated mirror mounts, and the accessibility of the entire system during electrical component changes.

The next phase of construction was the connection of Rogowski coils, current viewing resistors, and voltage dividers used to provide diagnostic information concerning the current through and voltage across various electrical components of the laser system. This information was necessary to determine the efficiency of the electrical circuitry in transporting the charge stored in the Marx generator to

the laser electrodes and trigger system. These diagnostics also provided information concerning the effectiveness of the double-discharge excitation system as a function of the gas flow parameters.

A resonant cavity alignment procedure was developed in an attempt to achieve CO_2 laser action. The ultimate objective was to operate the laser with the following output characteristics:

```
OUTPUT ENERGY PER PULSE - - - - - - - - -10-50 joules
PULSE TIME - - - - - - - - - -0.1 to 1.0 microseconds
PEAK OUTPUT POWER- - - - - - - - 10 megawatts minimum
MAXIMUM INPUT VOLTAGE- - - - - - - - - - 60 kilovolts
LASER EFFICIENCY - - - - - - - - 5-10 percent minimum
```

This paper reports the investigation of the operation and effectiveness of the double-discharge laser pumping technique. Primary emphasis was focused on the circuit element values and gas flow mixture ratio as parameters for producing an efficient discharge.

II. CONSTRUCTION

A. MECHANICAL

The basic physical dimensions and elements of construction
of the double-discharge laser box were previously reported
[Ref. 1]. The major modification to this element of the
system was the redesign of the laser box end plates and the
mounting portals for the NaCl windows. Two major problems
existed with the previous design. The NaCl windows are
subject to fogging being very hygroscopic. The previous
design required glueing the crystal to the end plate portal
in order to maintain the crystal in position as well as to
insure some amount of gas tight integrity. Upon fogging,
the crystal had to be detached from the portal, introducing
the possibility of scratching the crystal, and then repolished.
The discharge area of the laser was designed to have a gap
of six centimeters maximum. Originally the portals and end
plates would only accommodate a two centimeter gap within
the discharge area. To solve both of these problems, newly
designed end plates and crystal mounting portals were
fabricated and placed on the laser box (Figure 1).

In addition to the laser box, the laser system consisted
of the Tachisto Marx generator, the pulse shaping network
composed of passive electrical components, the D.C. power
supply and the gas flow system. A lucite platform was
erected above the laser box to reduce the length of the

wiring from the Marx generator to the pulse shaping circuit elements and finally to the laser box.

B. GAS FLOW SYSTEM

Although carbon dioxide is the gas which after sufficient excitation emits coherent radiation in a CO_2 TEA laser system, helium and nitrogen are also important in promoting efficient laser action. Investigations of double-discharge laser systems have shown that the preionization and glow discharge as well as the laser output power and efficiency are dependent upon the component ratio of the gas mixture [Ref. 2].

In order to precisely control the mixture ratio of helium, nitrogen, and carbon dioxide, each of the gases was reduced to 20 psi regulator outlet pressure prior to passage through individual gas flowmeters. The flow of each gas through the respective flowmeter into the mixing tank was controlled by a throttle valve.

The gas mixture was transported from the three liter mixing tank to the laser box via a one quarter inch plastic tube. The gas mixture was passed through a cartridge type filter (Matheson Gas Products, Model #450 with Model #451 cartridge) to insure that no oil, water, or particles larger than 12 microns entered the laser discharge cavity. The tubing was terminated with a "tee" connector such that the gas was introduced into one side of the laser box at three locations, each midway between the anode and cathode. Two

8

gas exhaust ports were located on the opposite side of the laser box. These one quarter inch exhaust ports were vented to the atmosphere through individual valves. This sytem (Figure 2) provided gas flow transverse to both the laser axis and the discharge path between the electrodes. A precise determination of the gas mixture ratio was based upon each flowmeter reading and the respective calibration charts [Ref. 3].

C. ELECTRICAL

A CO_2 TEA laser depends upon selective direct electron impact and molecule-to-molecule energy transfer for creation of the population inversion necessary for laser output. Both of these processes occur when the gas mixture of helium, carbon dioxide, and nitrogen is subjected to electrical breakdown between the electrodes within the laser cavity. Atmospheric pressure operation of a CO_2 laser is preferable to low pressure operation due to the greater molecular density and, therefore, greater available energy. To overcome the attendant problems of high pressure opera-tion transverse excitation must be achieved by modifying the electrode geometry. Transverse excitation implies a short discharge length but large discharge area to achieve the discharge volume necessary to excite the gas mixture, create a population inversion, and thus enable laser action to occur.

Transverse excitation is superior to longitudinal excitation since smaller working voltages are necessary to obtain a large discharge volume at atmospheric pressure. Another advantage is the inherent low impedance of a small electrode gap which allows rapid injection of the discharge excitation energy. For efficient laser operation, the excitation energy pulse must be short compared to the lifetime of the CO_2 molecule in the upper laser energy level. This time must be short so that collisional depopulation of the upper laser level does not occur during pumping.

A third advantage of the transverse excitation method results from the gain switching phenomenon. During the excitation phase of operation, the gain builds up to a large valve. Prior to rapid depopulation of the upper laser energy level the gain has reached a maximum with subsequent production of a giant pulse without Q-switching [Ref. 4].

Double-discharge preionization techniques must be used in conjunction with the transverse excitation method in order to attain uniform volume discharge [Ref. 5]. Preionization by the double-discharge configuration was accomplished through the use of 144 insulated trigger electrodes which were charged essentially to the same potential as the anode [Ref. 1].

A three-stage Marx generator (Tachisto, Inc., Model MC-3, No. 14) supplied with a negative voltage up to 20 kilovolts and 15 milliamps by an unregulated D.C. power

supply was used as the electrical power source for the break-
down. The Marx generator was used instead of a coupling
transformer. Since voltage multiplication was achieved
in the Marx generator, a lower charging voltage was used
to attain the 20 to 60 kilovolts required to produce the
atmospheric pressure breakdown between the laser electrodes.
In addition, the Marx system did not have to contend with
the hysteresis effect of the iron core in a transformer
which could increase energy leakage [Ref. 6]. The capaci-
tance per stage of the Marx generator was 0.5 microfarads
(with the possibility of increasing to 1.1 microfarads for
greater energy storage) producing an overall generator
capacitance of 0.167 microfarads during discharge. The
theory of the Marx generator operation and pulse repetition
rate restrictions were previously enumerated and remained
unchanged throughout this investigation [Ref. 1].

The uniform glow discharge produced by the double-
discharge system was an efficient pumping mechanism for
exciting the gas mixture. Glow discharge in the gas mixture
between the electrodes can be maintained by limiting the
discharge time such that it is short compared to the arc
formation time. Arc formation time is the sum of the
statistical and formative time lags. The time lapse be-
tween application of the static breakdown voltage and the
appearance of an initiating electron within the discharge
gap is defined as the statistical time lag. The double-

discharge system reduces this time lag by generating a uniform ionization layer near the cathode before the onset of the main glow discharge between anode and cathode. The formative time lag is defined as the time required for an arc streamer to propagate across the gap after the discharge has been initiated. For proper operation, it is necessary to generate a glow discharge in the large discharge volume then reduce the voltage enough to prevent arc formation. The operation of the electrical discharge system was characterized by a permissible operating region beyond which arcing was prevalent. When the system arced there was little chance of laser emission since all the energy was dumped through the narrow channel of the filamentary arc. This process heats the gas in the arc filament significantly, thereby populating the lower laser energy level resulting in no population inversion. The arc also reduces or eliminates the large volume glow discharge, further preventing the creation of a population inversion. In addition, arcing has been shown to scatter laser radiation within the laser cavity [Ref. 4]. The heating of the gas mixture due to arcing contributes to thermal defocusing of the radiation in the resonant cavity, further reducing the possibility of laser output [Ref. 7].

Control of the voltage rise time and decay time constants of the input energy pulse from the Marx generator to the laser cavity electrodes was effected through the use of the

passive circuit elements shown schematically in Figure 3.
This particular circuit configuration had been extensively
tested in an operating CO_2 TEA laser system with a similar
double-discharge excitation technique [Ref. 6]. Due to the
proven reliability of this circuit, it was used as the
basic configuration with the values of R_1, L_1, and C_2
variable. These parameters were varied during system testing
to determine the values which produced optimum preionization
and glow discharge within the cavity.

The circuit component designations used in the following
description of operation are those shown in Figure 3. C_1
is the storage capacitance of the Marx generator. Initially
C_1 was charged by the D.C. power supply and all other elements
were uncharged. When the spark gaps of the Marx generator
were fired, they acted essentially like the closing of a
switch. Before breakdown in the discharge gap, the anode-
cathode gap and trigger-cathode gap were capacitors of 93
and 1000 picofarads, respectively. Each of these two gaps
effectively became a parallel combination of a capacitor
and large resistance during the initial breakdown stage
when a very small current flowed. As breakdown continued
and an appreciable current began to flow, the resistance of
the gap decreased progressively to a very small value. The
$L_1 C_2$ combination was used to control the rise time of the
voltage pulse in the main (anode-cathode) gap. Decreasing
the initial slope of the high-voltage pulse allowed a slow-

rising trigger corona discharge current to uniformly preionize the main discharge volume. R_1 and C_1 established the high-voltage pulse decay constant which insured that the high-voltage across the main gap was reduced after initial breakdown enough to prevent arcing and at the same time remained high enough to extend the pumping time.

When the spark gap switch was closed, C_1 began to discharge. Current flowed through R_1 and L_1, thereby charging C_2, C_3, and the anode-cathode and trigger-cathode gaps. C_3 was much larger than the anode-cathode capacitance or trigger-cathode capacitance, yet smaller than C_2. The impedance of the anode-cathode gap was initially greater than the impedance of the trigger branch; therefore, initially the current flowed into the trigger branch of the circuit and a high voltage was impressed across the trigger-cathode gap. This voltage induced preionization and charged C_3. Subsequently, the main gap experienced electrical breakdown which reduced the voltage across the anode-cathode gap. During the previous processes C_2 was charged. When the main gap broke down, current flowed from C_1 and C_2 through the main gap. Current continued to flow in the main gap until the voltage was reduced below the static breakdown voltage.

D. RESONANT CAVITY

In addition to the population inversion of a lasing medium (e.g., CO_2 molecules), a resonant cavity consisting of two mirrors and the discharge volume of the laser cavity

is a requirement for laser output. The two mirrors form an
optical resonator. The mirror referred to as the rear
or back mirror must be totally reflecting or as nearly so
as possible. The forward or front mirror must be partially
transmitting to allow a fraction of the laser radiation
energy to escape as output. CO_2 TEA lasers have been
operated efficiently with front mirrors having a transmis-
sion coefficient of 0.10 to 0.30. Output coupling of the
laser radiation may be achieved by several methods. If a
solid-back material is used, it must have a transmission
coefficient sufficient to optimize output without damping
out the radiation within the cavity. A second method is
output hole coupling wherein output holes are drilled in a
solid, highly reflective mirror. The partially transmitting
method was not used due to the high cost of such mirrors.
Output hole coupling was used since this method is just as
effective as the partially transmitting mirror when used in
a high gain system and the hole size is small compared to
the mode spot size [Ref. 8].

The fully symmetric resonant cavity stability analysis
for the CO_2 TEA laser as originally constructed was previous-
ly developed [Ref. 1]. The resonant cavity was changed to
a half-symmetric stable resonator. A four-inch diameter,
copper mirror with three-meter radius of curvature replaced
the original gold-coated aluminum rear mirror. The front
mirror in the half-symmetric resonator design was a flat,

circular, polished copper plate with a 0.79 mm hole drilled
in the center to provide for output hole coupling of the
laser energy. Copper has a reflectivity of 98.8% for
radiation with wavelength of 10.6 microns [Ref. 9].

The "g" parameter of a mirror is defined as:

$$g = 1.0 - (L/R)$$

where R is the radius of curvature of the mirror. The
resonant cavity length (L) of the half-symmetric system was
150 cm. Consequently, the parameter g_1 for the back mirror
was 0.5 while g_2, the front mirror parameter, was 1.0. The
stable resonator condition ($0 \leq g_1 g_2 \leq 1$) was still satisfied
for the half-symmetric system.

The NaCl crystal windows were mounted at the Brewster
angle of 56°19' on either end of the laser discharge cavity
(Figure 1). A radiation beam traveling along the optic
axis of the mirror cavity is displaced upward in passing
through the Brewster angle windows. The upward shift must
be considered during the alignment of the mirrors to insure
that the major portion of the radiation will resonate between
the mirrors and in the middle of the discharge region. The
upward displacement of the beam may be calculated using the
geometrical relationships shown in Figure 4.

  d = upward vertical displacement of beam due
      to windows.

  θ_i = Angle between incident ray and normal to
      crystal face.

n_t = 1.4906, Index of refraction of NaCl for
radiation of 10.6 microns.

t = 0.952 cm, Average thickness of NaCl window.

h = distance between incident normal and
exit normal of crystal.

b = distance from inner crystal face to
radiation exit line extension.

θ_t = angle of refraction between incident
normal and ray direction through crystal.

n_i = 1.0 index of refraction of air.

$\tan \alpha = b/h$

$\tan \theta_t = h/t$

$\cos \alpha = d/t\text{-}b$

$d = (t\text{-}h\tan \alpha) \cos \alpha$

$d = (t\text{-}t \tan \theta_t \tan \alpha) \cos \alpha$

$\alpha = \pi/2 - \theta_i$

$\sin \alpha = \cos \theta_i$

$\tan \alpha = \cos \theta_i/\sin \theta_i$

$\tan \theta_t = \sin \theta_t/\cos \theta_t$

$d = t \sin \theta_i (1 - \cos \theta_i/n_t \cos \theta_t)$

As shown in Figure 1, the angle of incidence of radiation
on the inner face of the crystal window was 56°19', the
Brewster angle. Therefore,

$d = (.952)(.832)(.5513)$ cm

$d = 0.44$ cm.

A lucite alignment insert with an etched crosshair 0.44 cm below the laser discharge centerline was placed in each end plate after removal of the resonant cavity mirrors and NaCl windows. The radiation from a small He-Ne laser was directed axially along the CO_2 laser discharge cavity such that it intersected the lucite insert crosshairs at each end individually. This procedure insured that the aligning laser light was 0.44 cm below the discharge cavity centerline without displacement due to the inserts. Great care was exercised to insure that the aligning laser was not moved with respect to the laser discharge cavity throughout the remainder of the alignment procedure. After removal of the inserts, the front mirror was positioned using the adjustable mirror mount such that the He-Ne aligning laser light passed directly through the output coupling hole. This mirror was rotated about the horizontal axis until the circular diffraction pattern produced by the aligning laser light on the output coupling hole was completely symmetric. This symmetric diffraction pattern indicated that the front mirror was perpendicular to the aligning laser beam. The rear mirror was then positioned to have the diffraction pattern from the front mirror impinge on the center of the four-inch diameter face. The rear mirror was then rotated about both a horizontal and vertical axis to reflect the diffraction pattern directly back onto the output coupling hole of the front mirror. This procedure insured that the two mirror

faces were parallel to each other yet perpendicular to the laser axis. It also provided a direct method of positioning the mirror centers 0.44 cm below the discharge cavity center-line to correct for the displacement of the laser radiation due to the NaCl window.

III.   DISCHARGE DIAGNOSTICS

The investigation of the laser discharge necessitated the use of several different types of diagnostic devices and procedures. Measurement of the time dependent values of current through and voltage across the various pulse shaping circuit elements and laser electrodes provided data which was correlated to determine the relative efficiency of the system as a whole when the circuit and gas parameters were varied.

Current in the various circuit elements was measured using current viewing resistors (CVR) when ground connection of one terminal of the CVR was feasible. In circuit elements where ground connection of one terminal was not feasible, a current viewing probe (CVP) of Rogowski coil design was used. The CVR and CVP diagnostic elements were obtained from T and M Research Products, Inc., 129 Rhode Island NE, Albuquerque, New Mexico 87108.

The CVR (Model #SDN-414-01) had a resistance of 0.01 ohms, a bandpass of 300 MHz and a risetime of 1.2 nanoseconds. Output from the CVR (Figure 5) at a rate of 100 amps per volt was through a standard BNC UG-88/U connector via a 50 ohm terminated RG-58A/U coaxial cable. This voltage signal was the input for a Textronic Type 555 dual-beam oscilloscope equipped with a Type L amplifier unit.

The current probes (Figure 5) were flexible Rogowski coils used to measure the time rate of change of current.

When properly positioned, the CVP completely encircled the conductor. The CVP produced an output voltage proportional to the time rate of change of the encircled current, independent of both conductor geometry and current distribution. Output from the CVP is given by:

$$V_{out} = (1/S)\ (di/dt)\ .$$

In this equation di/dt is the rate of change of monitored current and S is the probe sensitivity. Probe sensitivity (S) was a function of probe mutual inductance, resistance, and load impedance [Ref. 10]. The CVP bandpass was typically about one MHz when operated into a 50 ohm terminated load. The probe output was via a 50 ohm terminated length of RG-58 A/U coaxial cable with a BNC UG-88/U connector. This voltage signal was the input for a Type O Textronics integrating amplifier module. Typical integrator resistance and capacitance values used were 0.1 megohms and 0.0001 microfarads which produced a 10 microsecond integration time. The electrostatic shield construction of the probe was a split copper foil wrap which was connected to the outer conductor of the cable.

Initially the voltage measurements were made using a 1000:1 series carbon resistor voltage divider. Poor response of the resistive voltage divider to the pulsed nature of the Marx generator discharge prompted a change to a capacitive voltage divider (CVD) designed for voltage

pulse measurement. The capacitive voltage divider provided 100:1 reduction of the voltage measured. A Textronics 10:1 resitive probe was used in series with the CVD to obtain 1000:1 voltage reduction prior to display on the oscilloscope.

The diagnostic wiring schematic shown in Figure 6 was determined to be the best operating condition for elimination of ground loop and other spurious signal detections super-imposed on the diagnostic measurements. The description of the diagnostic hook-up which follows is referenced to the schematic (Figure 6). The trigger generator chassis was isolated from the wall plug ground. The only ground connection for the trigger generator was through the Marx generator. An unregulated D.C. power supply provided from zero to a negative 20 kilovolts to the Marx generator. The "common" lead from the D.C. power supply to the Marx generator chassis provided electrical continuity during the charging phase of Marx operation. A 3/4 inch flat copper braid grounding strap from the Marx generator spark gap ground terminal to the building electrical conduit ground provided the only ground connection for the entire laser and diagnostic system. This one ground terminal connection was necessary to prevent ground loop currents from introducing spurious signals into the diagnostic measurements. The CVD was connected with the low side clipped to the single ground strap and the input terminal was connected to either the

anode or between the trigger capacitor (C_3) and the trigger bar. Anode voltage or trigger voltage was monitored depending on the position of this input lead.

Current viewing probes (CVP) were positioned as shown to monitor anode current and trigger current. It was necessary to insure that the current conductor was closer to the copper shield than the cable termination part of the CVP for accurate current measurements. The geometry of the positioning of the CVP was otherwise unimportant. A 50 ohm terminator was a requirement for impedance matching of the CVP to the oscilloscope. Two CVP's were used as shown. The CVP labeled "LS" had a sensitivity (S) of 195 amp/volt-μ sec while "MS" had a sensitivity (S) of 31 amp/volt-μ sec. An RC integration time of 10 microseconds was used with both CVP coils; therefore, the calibration was

MS	1 volt = 310 amps
LS	1 volt = 1950 amps

Current viewing resistors were positioned with one terminal directly connected to the ground terminal of the Marx generator spark gaps and the input terminal connected to either the pulse shaping resistor (R_1) or a 3/4 inch copper braid strap attached directly to the laser cathode. An impedance matching 50 ohm terminator was used between the CVR coaxial cable lead and the oscilloscope.

The two oscilloscopes were placed in an aluminum screen enclosure in close proximity to the laser and electrical

component platform. RG-58 A/U coaxial cable has an average capacitance of 30 picofarads per foot; thus, no additional coaxial leads could be used with the CVD other than the lead which was an integral part of the 10:1 attenuation probe.

In addition to the aforementioned requirements on physical placement of the diagnostics, the combination of diagnostic inputs to a dual-beam oscilloscope had to be controlled. If one CVP coil input and either a CVR or voltage divider input were both connected to the same dual-beam oscilloscope, ground loops were set up introducing spurious signals on the diagnostic data recorded on the Polaroid pictures of the scope traces. A CVR and a voltage divider could both be input for the same dual-beam scope without distortion of the signal. Two CVP coil inputs were also acceptable on the same scope without introducing distortion of the signal.

All of the above procedures were followed to produce the most accurate distortion-free diagnostic data traces possible for investigation of the double-discharge process of gas mixture excitation.

IV.   RESULTS OF DISCHARGE INVESTIGATION

A.   PLASMA PROPERTIES

The diagnostic devices and operating procedures discussed in section III were used to obtain oscilloscope voltage traces which were recorded on Polaroid film for subsequent analysis. A reproduction of a typical scope trace is shown in Figure 7 indicating the representative values of anode-cathode voltages and current during a normal glow discharge of the laser. It should be noted that the voltage maximum leads the current maximum in this sketch. It was previously stated that the laser electrodes formed a capacitor with a measured capacitance of 93 picofarads. During discharge the electrodes may be viewed as a capacitor with a parallel resistance of ever decreasing value allowing more and more discharge current to flow. The phase difference of the voltage and current in the typical discharge, however, indicates that an inductive effect was present. This inductive effect was due to either a real inductance of the plasma created between the laser electrodes or a spurious effect of the diagnostic voltage divider. If the inductive effect was due to the voltage divider, then all subsequent energy and power calculations were conservative due to the peak shift of the current. If the inductive effect was plasma-produced then the plasma was acting as a circuit element with resistance and inductance properties. The

voltage across such a circuit element is given by:

$$V = I\Omega + L \, di/dt$$

where Ω is the resistance of the plasma and L is the plasma
inductance. Rough calculations indicated that the plasma
inductance would have to be on the order of microhenries
to produce a phase shift of this magnitude.

B. GAS MIXTURE DEPENDENCE

During the course of the investigations many different
gas mixture ratios were tested as to the influence each
had on the discharge characteristics. Of prime concern
were the values of anode-cathode voltage and current which
ultimately indicated the energy transferred from the Marx
generator to the gas. The effect of various percentages of
helium in the gas mixture on the peak anode-cathode voltage
and current is shown in Figure 8. The decrease in peak
voltage as helium percentage was increased should be
noted. The decrease in discharge voltage may be explained
as follows. The resistivity of the partially ionized gas
mixture decreased as helium percentage was increased.
A leakage current of approximately 30 amps flowed from the
exposed trigger wires to the cathode during operation at
high helium percentages. Possibly the anode-cathode voltage
was limited by this weak breakdown process between the
trigger wires and cathode. This problem is further discussed
in Section IV-E.

26

The interelectrode plasma resistance (Ω), a calculated
parameter, was also of importance in describing the effect
of helium percentage on the discharge characteristics.
This resistance was calculated using the measured anode-
cathode voltage divided by the measured anode-cathode
current. Due to the phase shift inherent in the voltage
and current traces, two different values of Ω were
calculated.

Ω_p = peak voltage/peak current

Ω^* = voltage at time current reaches peak value/
peak current

Figure 9 indicates a slight variation in the calculated
value of the resistance of the discharge with increasing
helium percentage. It should be noted that at lower helium
percentages there was no variation. This slight variation
at high helium percentages indicated that only a small error
in the interelectrode plasma resistance calculation could
have been introduced by the phase shift.

The implications of the discharge resistance calculations
will be shown by an order of magnitude calculation. If the
discharge was assumed to be relatively uniform over the
entire cathode area then:

$$\eta = \Omega \ A/L$$

where η is the discharge resistivity, L is the gap distance
between the electrodes, and A is the cross-sectional area

27

of the discharge. The maximum measured electron density
in the TEA laser discharge is approximately 10^{13} electrons
per cubic centimeter. Such densities were measured in
E-Beam TEA lasers. Typical measured electron density in
TEA lasers operating at 8:1:1 (He:CO_2:N_2) gas mixtures is
between 10^{10} and 10^{11} electrons per cubic centimeter [Ref.
11]. Neglecting coulomb collisions at such a low degree
of ionization, electrons can lose energy in the following
types of encounters:

    1.   Elastic collisions with N_2, CO_2, or He.

    2.   Inelastic excitation of CO_2 or N_2.

    3.   Ionizing collisions with N_2 or CO_2.

The plasma resistivity (η) may be written as:

$$\eta = M_e \, \nu_{eff} / n_e \, e^2$$

where M_e is the electron mass, n_e is the electron density,
e is the electron charge, and ν_{eff} is the effective rate of
momentum transfer collisions for a single electron. ν_{eff}
is given by:

$$\nu_{eff} = n_s \, \sigma \, v_e$$

where $\sigma \, v_e$ is the rate constant for the process of interest.
In order to determine the plasma resistivity (η), it was
necessary to calculate an order-of-magnitude estimate of
ν_{eff}. The cross-section information for the collisions
of interest were taken from Figures 10 and 11. Figure 10
illustrates the elastic scattering probability of collision

28

from which the elastic scattering cross-section may be
calculated. Figure 11 is a graph of inelastic scattering
rate constants (σv_e) and single ionization rate constants
as a function of electron temperature in electron volts.

An electron temperature of 2.5 e.v. was assumed. Such
a high electron temperature may be expected when operating
at high helium content (90%-95%). This value was also
chosen to avoid the elastic scattering resonances which
occur for CO_2 and N_2 near 1.5 e.v. to 2.0 e.v. P_c is
defined as the probability of collision at a pressure of
one torr. The elastic scattering cross-section (σ) was
obtained from P_c by the following relation:

$$\sigma = 2.83 \times 10^{-17} P_c .$$

σ has units of square centimeters. An electron with an
energy of 2.5 electron volts has a speed of approximately
9×10^7 cm/sec. The effect of each collision process on
electron momentum was the main interest in the resistivity
calculation. Perhaps the inelastic collision processes
should be weighted more than others in the calculation of
ν_{eff}. Since an accurate weighting procedure was not clear
and only order-of-magnitude numbers were desired, an attempt
to weight the various terms was not made. Therefore, the
effective rate of momentum transfer collisions (ν_{eff}) was
determined to be:

$$\nu_{eff} = n_{He} \ (4.3 \times 10^{-8}) + n_{CO_2} \ (8.0 \times 10^{-8} +$$

$$3.0 \times 10^{-9} + 7.0 \times 10^{-9} + 2.0 \times 10^{-13}) +$$

$$n_{N_2} \ (8.5 \times 10^{-8} + 3.0 \times 10^{-8} + 4.0 \times 10^{-11})$$

where n_S represents the density of the species in question with units of cm^{-3}. In the terms above it is clear that elastic scattering processes dominate the determination of ν_{eff}. Therefore, ν_{eff} is given approximately by the following:

$$\nu_{eff} = n_{He} \ (4.3 \times 10^{-8}) + n_{CO_2} \ (9.0 \times 10^{-8}) +$$

$$n_{N_2} \ (11.5 \times 10^{-8}) \ .$$

ν_{eff} is approximately $1.1 \times 10^{12} \ sec^{-1}$ for a typical operating condition of 95% helium, 4.2% carbon dioxide, and 0.8% nitrogen. At this operating condition a typical value for Ω during the discharge was 15 ohms. Substitution of this value into the expression for resistivity

$$\eta = \Omega \ A/L$$

where A is 0.09 m^2 (cathode surface is 90 cm x 10 cm) and the gap length (L) is 0.02 m, results in a value of 67.5 ohm-meters for η. Rearranging the theoretical expression for η and solving for the electron density during the discharge yields an electron density of $5.8 \times 10^{11} \ cm^{-3}$ for the 95% helium operating condition. The same calculations for an operating condition of 79% helium, 16.5% carbon

dioxide and 4.5% nitrogen result in a value for ν_{eff} of

1.4×10^{12} sec^{-1}. For this operating condition Ω was 70

ohms during discharge. Thus, the electron density was

approximately 1.6×10^{11} cm^{-3}. The calculated value of

electron density in the discharge was not very different

from the expected value of 10^{10} to 10^{11} cm^{-3} for a TEA

laser operating with 80% helium. This was an encouraging

result. Nevertheless, such a crude calculation could be

used only to indicate the order-of-magnitude of electron

density in the discharge. The assumptions which may have

introduced error into the calculations of electron density

are listed below:

    1. A uniform discharge covering the entire cathode

surface was assumed in using the expression:

$$\eta = \Omega \, A/L \ .$$

A smaller effective discharge area would cause the previously

calculated resistivity to be overestimated and thus the

previously calculated electron density would be underestimated.

    2. A constant electron temperature (T_e) was assumed in

the calculations. It was quite clear from experience in

operating the discharge that the electron temperature was

a reasonably sensitive function of the gas mixture. In

the regime of 1.5 to 2.0 electron volts the CO_2 and N_2

elastic scattering cross-sections exhibit resonance effects

which can increase the scattering cross-sections by factors

of two or three.

3. The inelastic processes were not given proper weight. Certainly these processes are important in the energy balance of the laser discharge; however, the inelastic processes were essentially ignored since the unweighted cross-sections were an order-of-magnitude smaller than the elastic scattering cross-sections.

The interelectrode resistance (Ω) provided a convenient parameter for describing the characteristics of the discharge as a function of gas mixture ratio. The resistance was determined as a function of time by calculating the quotient of the voltage and current measured at the same time for several discharge firings. It was previously shown that the phase shift of current and voltage peaks did not significantly affect the relative resistance calculations; thus, assuming a strict time dependence did not introduce a large error in describing the plasma resistance.

Figures 12 and 13 illustrate the dependence of the resistance on the helium percentage as a function of time for several firings as indicated. Comparison of the two figures indicates that as the helium percentage increased, the time period of low resistance (referred to as the "window" in this paper) also increased. If these curves are viewed in three dimensional space with coordinates: resistance, time, and helium percentage, a curved surface of increasing resistance with decreasing percentage of helium would be evident.

The peak power and energy dumped into the discharge from the Marx generator were calculated using a Hewlett-Packard, Model 9810 A, calculator from the voltage and current versus time data traces. The energy dumped into the discharge is found to increase as the helium percentage increases as shown in Table I. The calculated numbers presented are reliable to within 20%.

TABLE I

Discharge Energy at Various Helium Percentages

% He	E (joules)
95.0	3.50
90.0	3.45
85.5	3.63
83.7	2.99
79.0	1.88
74.0	1.28

R_1 = 5.6 ohms C_2 = 0.008 μf

L_1 = 7.9 μh C_3 = 0 μf

V_o = 22.5 KV

In order to test the influence of increased nitrogen in the gas mixture, the flowmeters for CO_2 and N_2 were switched. This arrangement permitted use of a gas mixture ratio largely composed of helium and nitrogen instead of being helium and carbon dioxide rich.

The minimum resistance of the discharge at a constant helium percentage was found to be smaller by a factor on the

order of two for the helium-nitrogen rich mixture than for the helium-carbon dioxide rich mixture. Conditions to be compared are grouped in Table II.

TABLE II

Plasma Discharge Resistance (Ω) and Corresponding Gas Mixture Ratio

				Circuit Parameters		
Ω	% He	% CO_2	% N_2	R_1(ohms)	L_1(μh)	C_2(μf)
13.0	88.8	2.6	8.6	3.7	11.5	0.016
39.7	88.8	8.9	2.4	5.6	7.9	0.008
28.6	83.0	2.9	14.1	3.7	11.5	0.016
53.0	83.0	13.7	3.3	5.6	7.9	0.008
52.9	80.0	3.3	16.7	3.7	11.5	0.016
65.7	80.0	15.8	4.2	5.6	7.9	0.008

This reduction of resistance was possibly due to the following effects. When the high triatomic (CO_2) molecular density was replaced by a high diatomic (N_2) molecular density, the accelerated preionization electrons have fewer inelastic collisions. Fewer inelastic collisions allowed the electrons to have a higher temperature for a given value of electric field divided by gas mixture pressure (E/p) as shown in Figures 14 and 15. A higher electron temperature implies a decreased elastic scattering cross-section, thus reducing electrical resistance (Figure 10).

It should be noted that in the data of Table II the circuit parameter $R_1 C_m/\tau$ is not constant; however, it will be shown in Section IV-C that plasma resistance was not strongly sensitive to variation in this parameter.

It was also determined that flow rate of the gas mixture had no effect on the values of current and voltage when all other discharge parameters were held constant. The helium percentage was the most important gas mixture parameter which determined the operating regime of the double-discharge system with all other parameters constant.

C. VARIATION OF PULSE SHAPING CIRCUIT RESISTOR

Resistor R_1 served three functions in the laser electrical circuitry shown in Figure 3. It helped shape the voltage pulse presented to the anode-cathode gap. It served to reduce the second peak of the voltage pulse to avoid a glow to arc transition late in the discharge. The resistor also acted as a safety resistor by providing a conducting path such that when the Marx generator was fired without subsequent discharge between the electrodes all of the energy was not dumped into the Marx charging resistors. Resistance (Ω) as a function of a normalized parameter $(R_1 C_m/\tau)$ is shown for a variety of discharge conditions in Figure 16. R_1 is the value of the safety resistor. C_m is the capacitance of the Marx bank. τ is the time necessary for the discharge current to reach its peak. Figure 16 shows that in the operating regime

(0.5< R_1C_m/τ < 1.2) that Ω does not vary strongly with R_1C_m/τ. Outside this operating regime undesirable effects predominate. At high values of R_1C_m/τ arcing is prevalent. At low values of R_1C_m/τ the discharge is very weak and Ω is quite large.

A representative curve of Ω as a function of time for a particular value of R_1 is shown in Figure 17. The shape and order-of-magnitude of $\Omega(t)$ were relatively insensitive to the value of R_1. This one representative curve (Figure 17) illustrates the operating regime "window" of low Ω to be about two microseconds wide.

Although the discharge resistance (Ω) was relatively insensitive to variations in the value of R_1 the energy coupled into the gas discharge was increased appreciably by an increase in R_1. This is shown quite well in Table III. For the three values of R_1 shown the values of Ω for the plasma were the same to within experimental error. It should be noticed that as R_1 is increased the fractional increase in second peak values of current and voltage are much larger than the fractional increase in first peak values. This is, of course, to be expected. Resistor R_1 and Marx generator capacitance C_m determine the decay envelope of the voltage pulse from the Marx generator. As R_1 is increased the slope of the decay envelope decreases allowing the second peak values of current and voltage to increase significantly.

TABLE III

Energy and Power with Pulse Shaping Resistor R_1

R_1	$R_1 C_m/\tau$	$I_{1st\ peak}$ (X 10^2 Amps)	$I_{2nd\ peak}$ (X 10^2 Amps)	$V_{1st\ peak}$ (KV)	$V_{2nd\ peak}$ (KV)	E (joules)	P_{peak} (X 10^6 watts)
5.83	.750	9.2	1.80	13	4.5	7.26	11.04
7.20	.923	9.3	2.50	17	7.0	10.05	13.20
8.90	1.140	11.0	3.25	14	7.5	10.30	14.30

L_1 = 7.9 μh C_2 = 0.016 μf

95% Helium

D. SYSTEM LIMITATIONS

The primary goal for the electrical circuitry and double-discharge system is to dump as much of the available Marx generator energy as possible into the gas discharge without arc formation. Once the energy is in the discharge the plasma acts very efficiently to couple the energy into electromagnetic radiation at 10.6 microns. A typical operating CO_2 TEA laser of similar design coupled 30% of the discharge energy into laser output power [Ref. 6]. Table IV compares the energy and power lost to the resistor R_1 with that dumped into the discharge for two representative firings.

E_R and P_R are the energy and peak power supplied to the resistor R_1. E_D and P_D are the energy and peak power delivered to the laser discharge. The calculated values for energy dissipated in the resistor and discharge are anticipated to be accurate only to within 20%. Table IV shows that almost all of the energy stored in the Marx generator was lost in resistor R_1 with only a small percentage coupled into the discharge. Efforts were made to increase the energy to the discharge. Changing the value of current rise time by variations of L_1 and C_2 (Figure 3) had the effect of increasing the discharge energy by approximately 20%, but clearly a more significant increase was required. An increased value of Marx capacitance C_m did increase the discharge energy, but only by increasing the total energy available (Table V); efficiency in fact decreased. Although

TABLE IV

Discharge System Energy Distribution

R_1 (ohms)	E_R (joules)	P_R peak (X 10^7 watts)	E_D (joules)	P_D peak (X 10^7 watts)	C_{marx} (µf)
9.00	21.6	3.2	9.8	1.2	0.167
4.56	99.6	9.6	14.8	1.0	0.367

increasing the percentage of helium in the gas mixture increased the energy, there is an upper bound where all the CO_2 is excluded; thus the system no longer has the possibility of being a carbon dioxide laser. Increasing the value of resistor R_1 and Marx generator discharge voltage increased the energy; however, there was an upper limit which when exceeded the system arced. The inability to couple energy efficiently into the laser discharge is the single greatest obstacle to successful laser operation. This problem will be further discussed and possible solutions will be presented.

One boundary to the discharge operating regime in parameter space is formed by those conditions for which arc formation occurs in the discharge. As a limiting boundary to laser operation arc formation is of interest. A graph of Ω as a function of time for a typical discharge in which an arc was formed is shown in Figure 18. The arc formation time indicated on the graph is typical of many of the experimental firings which produced an arc. Maximum intensity of the arc was defined to occur at the time of maximum current flow after arc formation. The discharge resistance (Ω) was less than one ohm (too small to measure) at that time. It is instructive to compare Figure 18 with Figure 17, a graph of resistance (Ω) as a function of time for a non-arcing discharge. The increased resistance at later times in Figure 17 indicates cessation of the glow discharge.

Arcing limits to the double-discharge operating regime
are tabulated in Table V. There are three parameters of
interest: $R_1 C_m/\tau$, % He, and V_o (initial voltage on the Marx
bank).

TABLE V

Limits of Double-discharge System Operating Regime

$R_1 C_m/\tau$	% He	V_o (KV)
1.36	97	22.5
1.29	95	22.5
1.19	85	22.5
0.895	95	27.0

Due to the statistical nature of arc formation, these
values are an average upper limit experimentally determined
from a large number of firings which resulted in arcs.
For the parameters $R_1 C_m/\tau$ and V_o laser operation is limited
at high values by the tendency toward arc formation; at
low values operation is limited because no discharge is
formed. For the remaining parameter (% He), laser operation
is limited at low values by the tendency toward arc forma-
tion. At high values of helium percentage discharge condi-
tions are ideal, but no advantage is gained if the CO_2
content is limited too severly. Thus a compromise must be
made between good discharge conditions and active molecule
(CO_2 and N_2) content. The improvement of discharge conditions

with increased He content is attributable to the higher
electron temperature achieved in the discharge. The higher
electron temperature enhances electron diffusion in the
discharge making the discharge more uniform and thereby
reducing the tendency toward arc formation.

Others have noted a high probability of discharge
arcing when firing the first one or more discharges of the
double-discharge system in an experimental period [Refs.
13 and 14]. This same tendency to arc on first firing was
noted in the system investigated. The solution to this
first shot tendency to arc was to extensively purge the laser
cavity with 100% helium for approximately seven minutes.
This tendency toward first shot arcing was possibly a
result of water vapor and other heavy molecules contained
in the air which leaked into the cavity when the system
was not in operation. Figure 14 indicates that for an E/p
of 10 volts/cm-torr (a typical operating condition) the
electron temperature in water vapor is very low. This lower
electron temperature inhibits electron diffusion allowing
the formation of a constricted arc.

E. PROBLEMS IN LASER DISCHARGE OPERATION

As discussed earlier the major obstacle to laser operation
has been the inability to couple a large fraction of the
stored energy into the gas discharge. This problem has been
analyzed and deserves further discussion. Figure 19 is a
comparative plot of power delivered to the safety resistor

(P_R) and power delivered to the discharge (P_d) for a typical condition in the operating regime. For this condition approximately 99 joules were delivered to R_1 while only 15 joules were delivered to the discharge. One notices at a glance that before P_d reaches its peak at 1.2 microseconds most of the stored energy has already been lost to R_1. The loss of this energy to R_1 could be reduced by either of two procedures:

(1) R_1 could be increased;

(2) R_1 could be eliminated completely.

Increase in R_1 will cause discharge arcing, unless the arc formation time in the gap can be increased. Preparations have begun to increase the electrode gap to four and then to six centimeters. This modification will give significantly longer arc formation times and should result in greater laser efficiency. Elimination of the safety resistor would require the installation of a timing circuit designed to "crowbar" the discharge before the arc formation time. At present there are no plans to install the crowbar circuitry.

In addition there is another problem limiting laser operation. Comparison of laser discharge voltage for conditions of differing helium content show that at high helium percentage the discharge voltage is appreciably reduced. Such a condition could occur if the trigger wires are not sufficiently insulated from the cathode electrode. Insufficient insulation would lead to a resistive leakage current

43

from the trigger wires to the cathode, thereby shorting the capacitive trigger voltage. Evidence that such a weak breakdown process (from the trigger wires to the cathode) actually occurs is presented in Figures 20 and 21. Presented are plots of trigger current versus time for helium percentages from 74% to 100%. Trigger voltage traces at 74% helium and 100% helium are also presented.

At 74% helium the voltage and current traces are reasonably close to being 90° out of phase. The current oscillations appear capacitive; if there is a leakage current from trigger to cathode it is small. At 79%, 83%, and 90% helium, the disappearance of the second positive trigger current peak is clearly evident. This is due to drainage of the trigger wire charge through the anode during discharge as expected. At 95% and 100% helium, however, the trigger current appears increasingly in phase with the trigger voltage and the positive trigger current dominates. This is direct evidence of a leakage current from the trigger wires to the cathode. Notice also that the trigger voltage at the high helium percentage is less than one-half the voltage at 74% helium. This also indicates that the voltage may be shorted by a weak breakdown from the exposed trigger wires to cathode. Plans are presently underway to better insulate the trigger wires from the cathode electrode. It is expected that this modification will increase discharge current, discharge voltage and provide a more efficient pre-ionization at high helium content.

There is one apparent problem in the operation of the laser discharge for which an immediate solution is not evident. At "low" helium percentage the resistivity of the discharge is greater than that for similar double-discharge lasers. At 74% helium the laser discharge under investigation demonstrated an $\eta = 6.4 \times 10^4$ ohm-cm. A similar double-discharge laser built by Pan UCRL [Ref. 6] demonstrates an $\eta = 2.7 \times 10^3$ ohm-cm at 71% helium. The UCRL laser operates at a similar E/p, but its discharge gap is five cm instead of two cm. At present it is not clear how the resistivity should scale with discharge voltage and dimensions. Thus it is not clear whether this order-of-magnitude discrepancy in η is due to improper laser design or merely due to the difference in operating regimes.

FIGURE 1

47
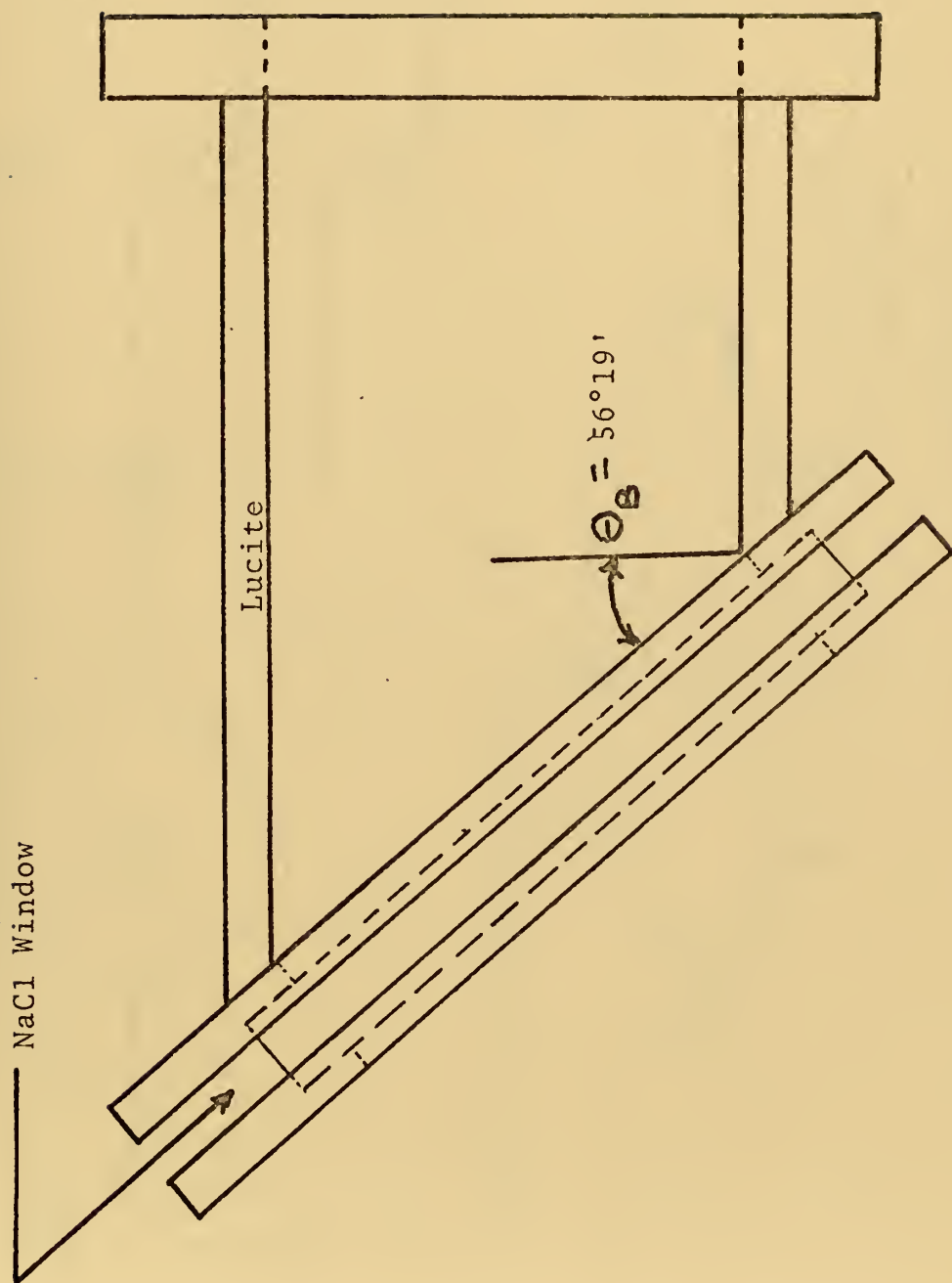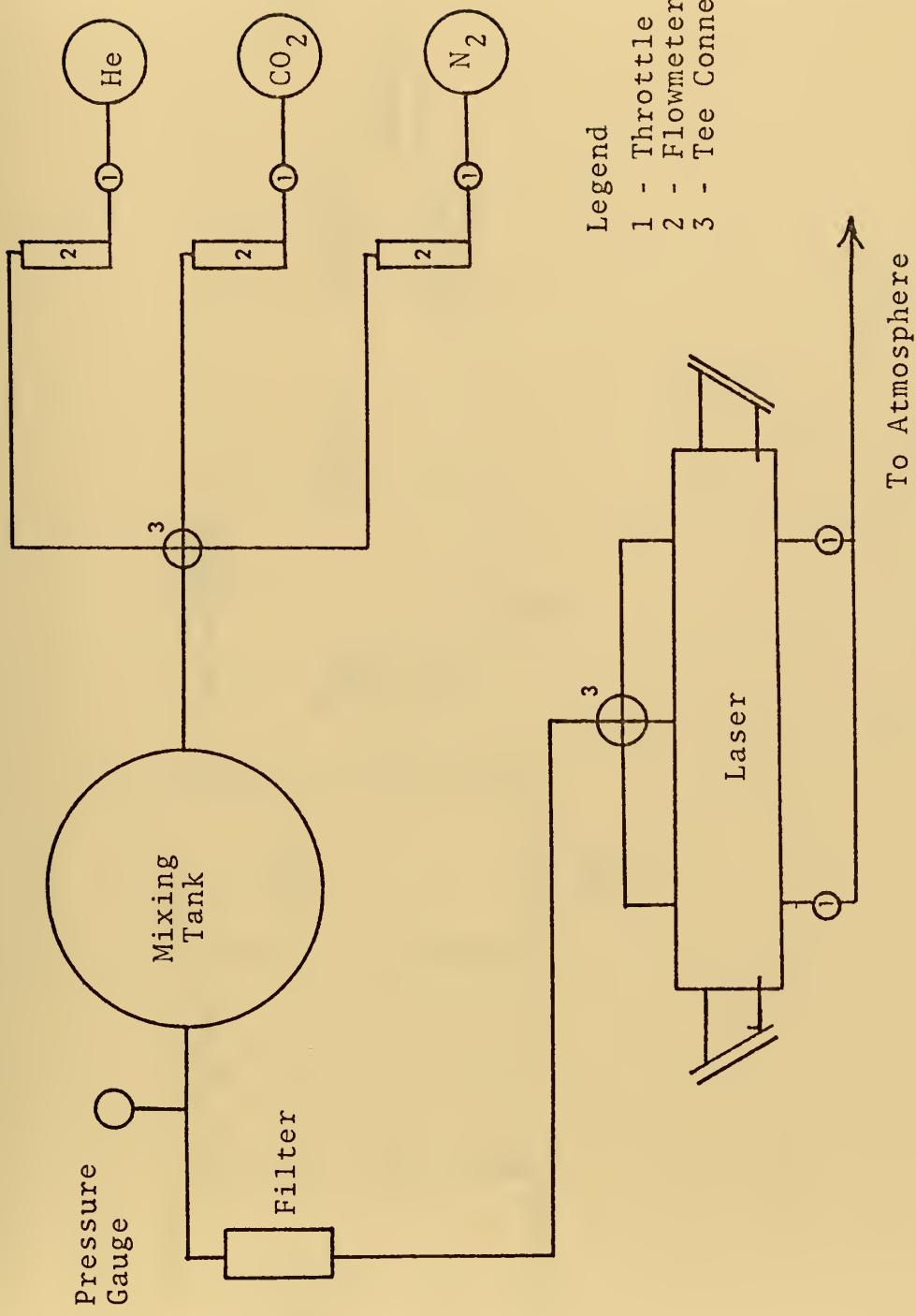
Legend
1 - Throttle Valve
2 - Flowmeter
3 - Tee Connector

GAS FLOW SYSTEM
FIGURE 2
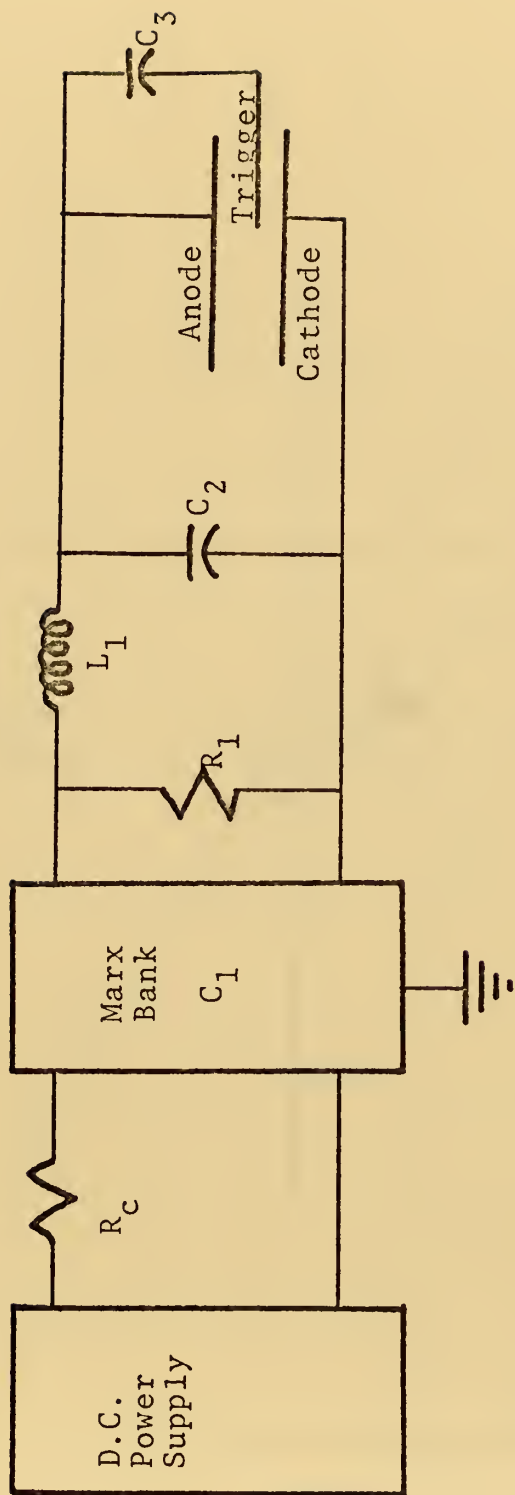
ELECTRICAL CIRCUIT

FIGURE 3

48
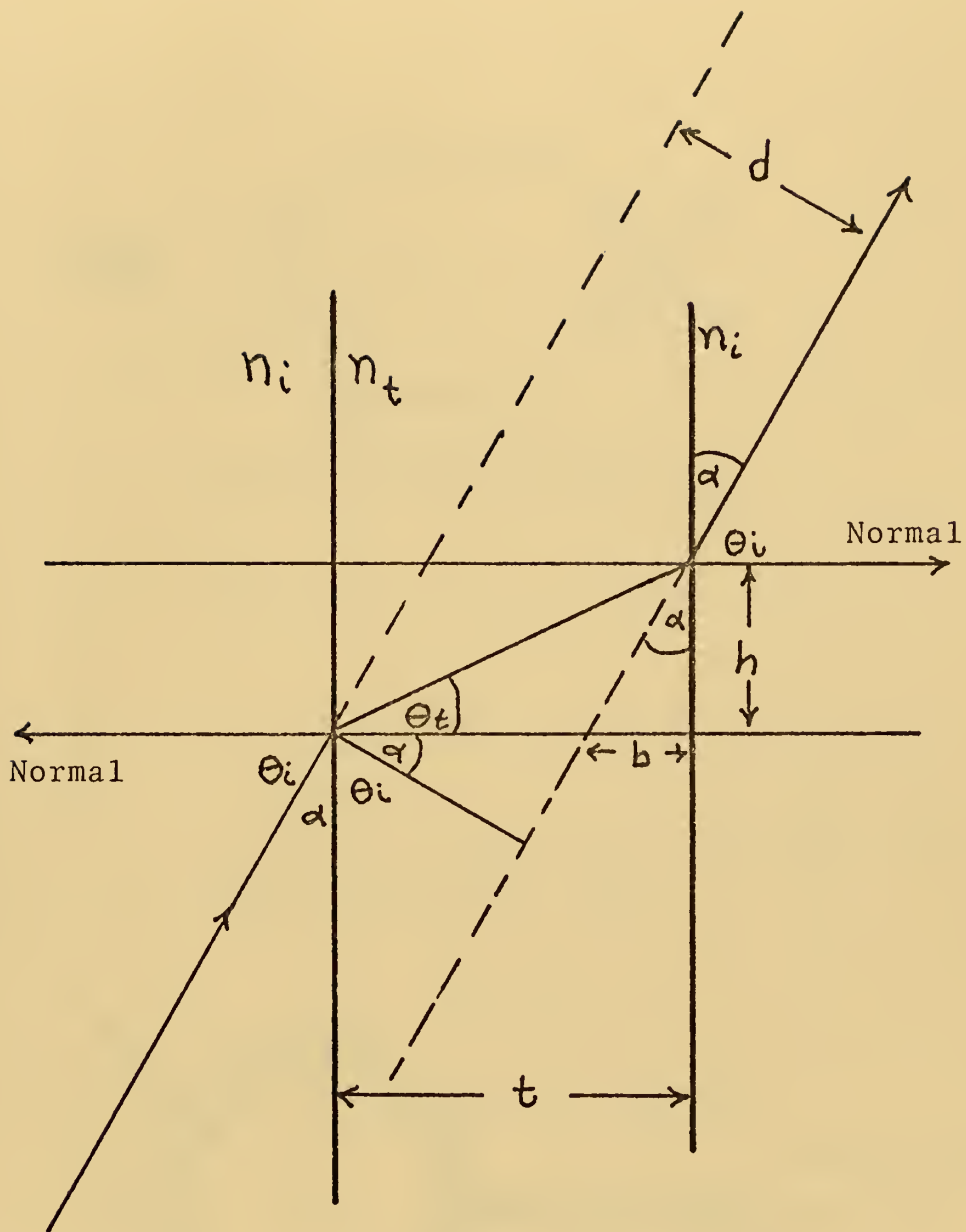
RADIATION BEAM DISPLACEMENT

(RAY PATH)

FIGURE 4

BNC Connector

Model SDN-414

Current Viewing Resistor

Current Viewing Probe

Split Shield

Oscilloscope
Input

Z

I
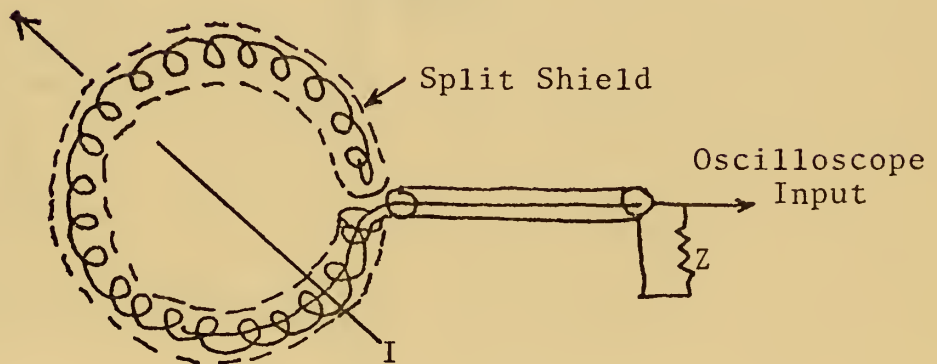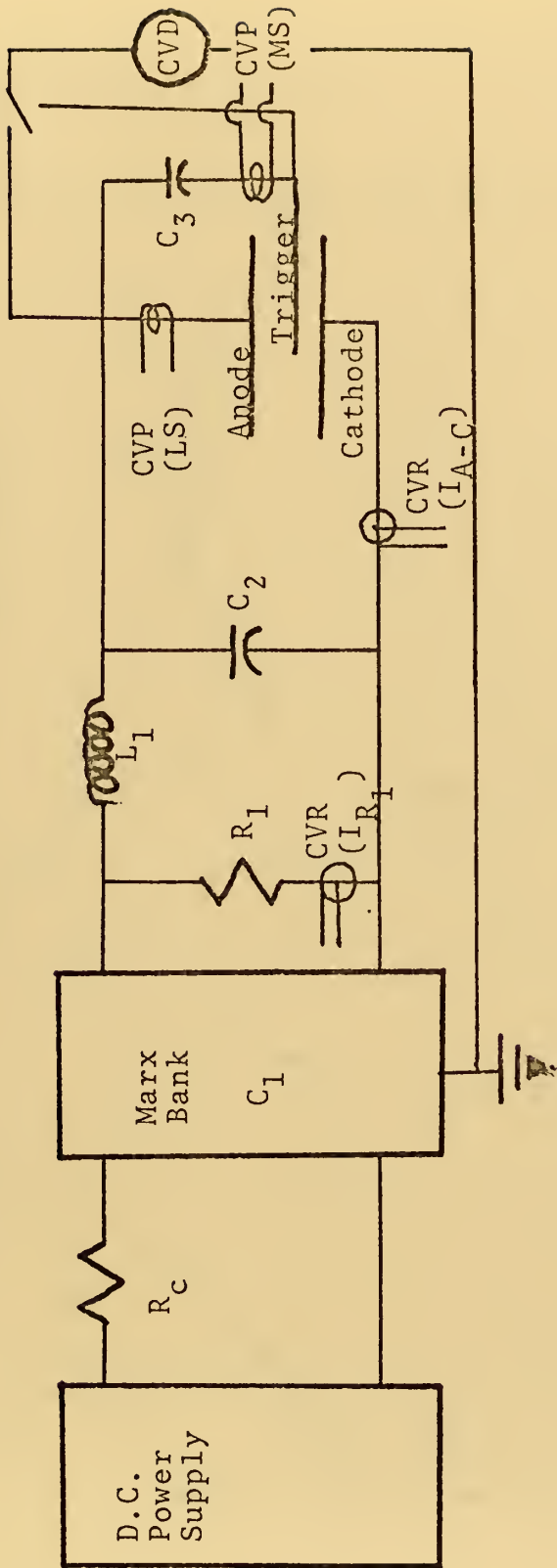
FIGURE 5

DIAGNOSTIC PLACEMENT

FIGURE 6

51

FIGURE 7

52

Peak Discharge Voltage
(Kilovolts)

Shots 2-7 3 Nov 1972
$R_1 = 5.6 \ \Omega$ $C_2 = 0.008 \ \mu f$
$L_1 = 7.9 \ \mu h$ $C_3 = 0$

Voltage

Current

Helium Percentage

FIGURE 8

Peak Discharge Current
(X 10^2 Amps)

53

FIGURE 9

54
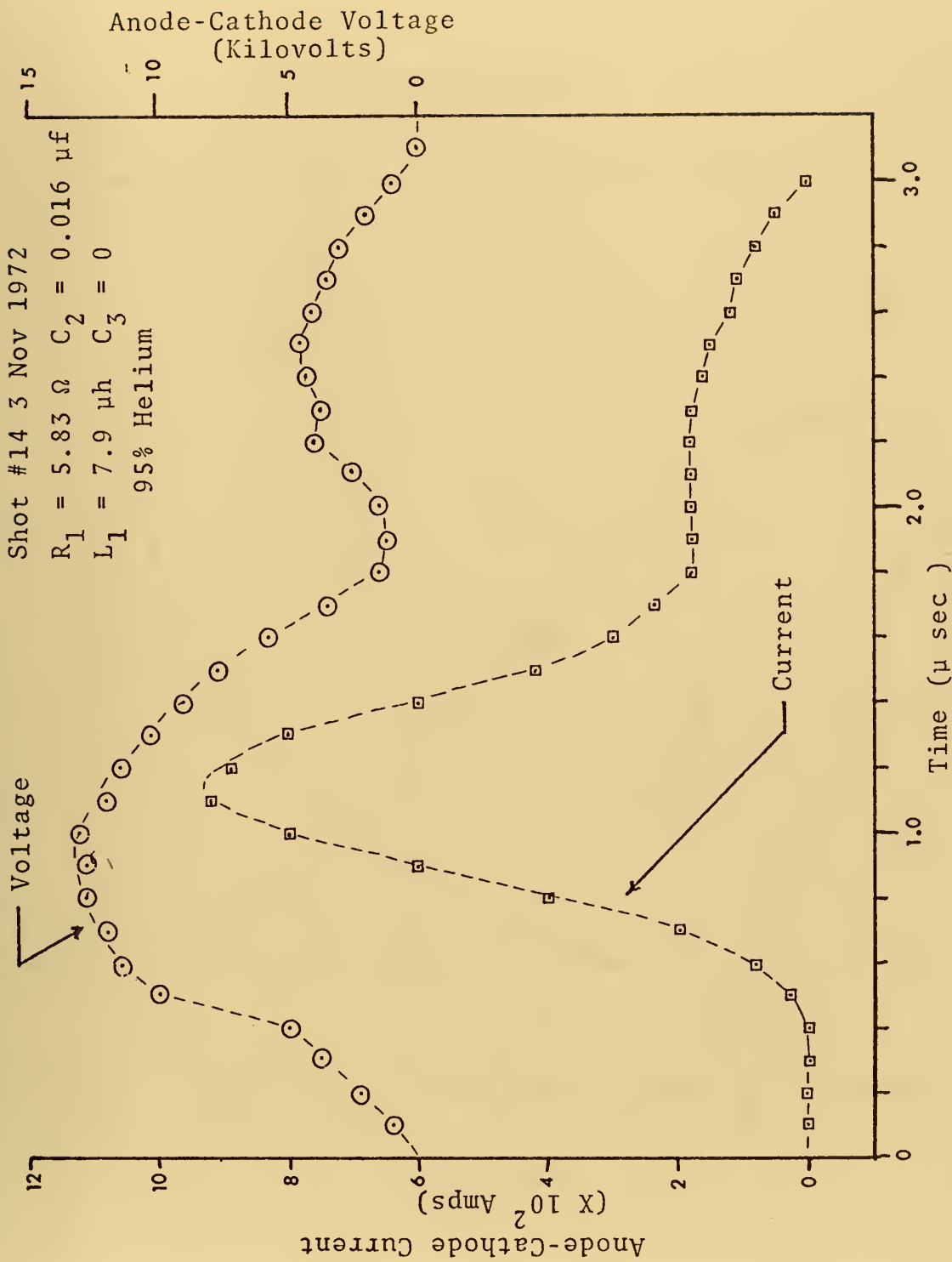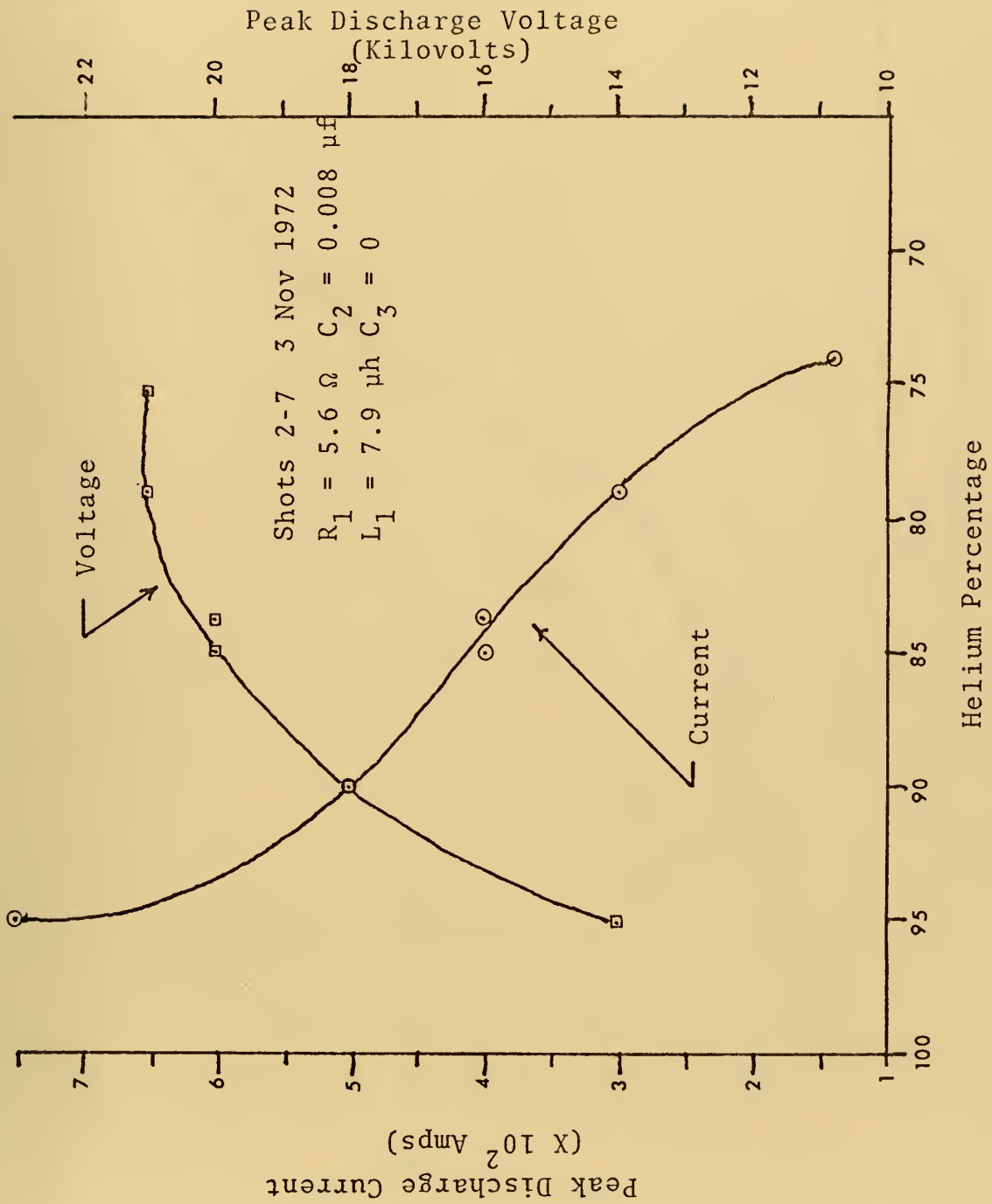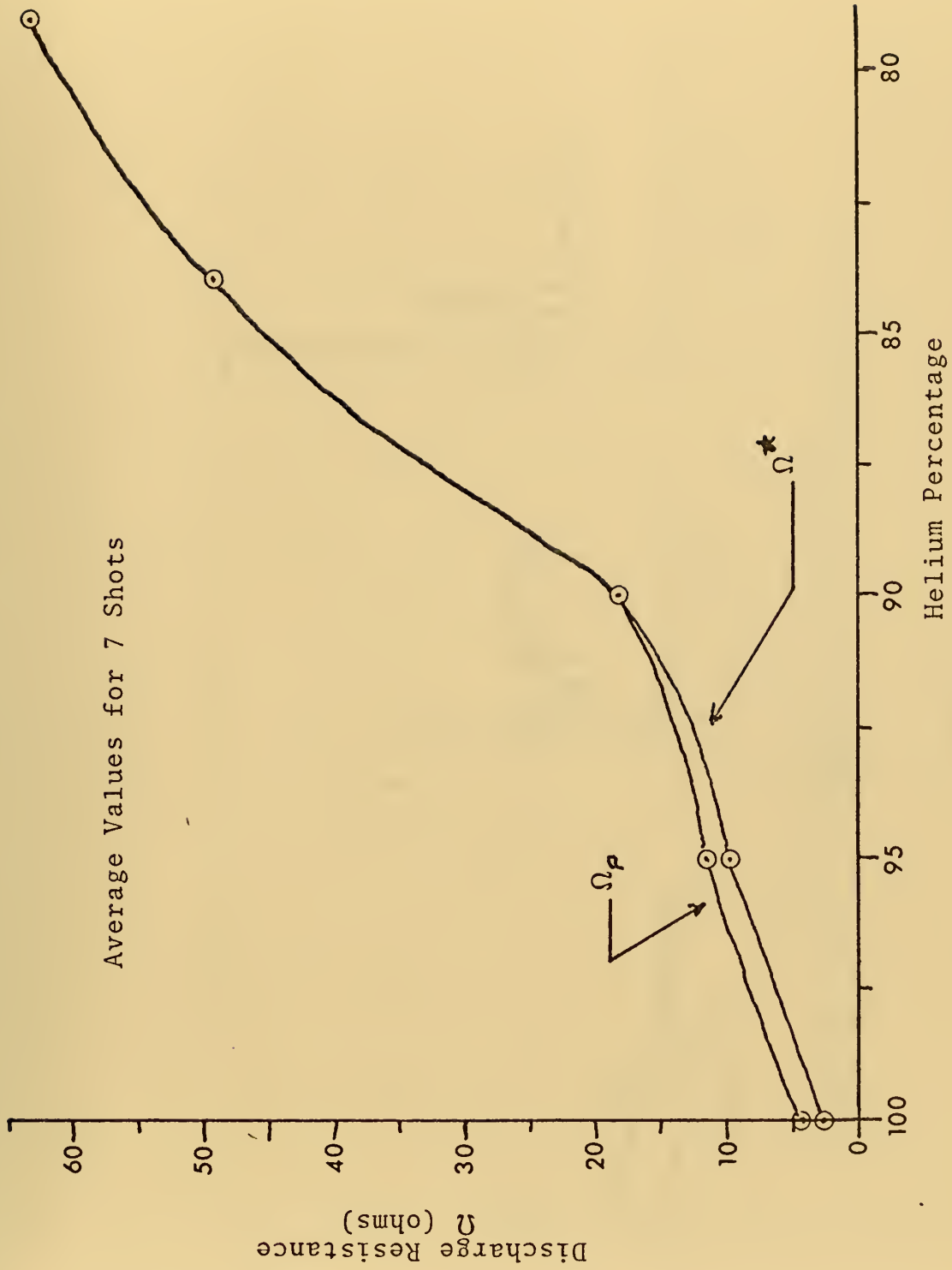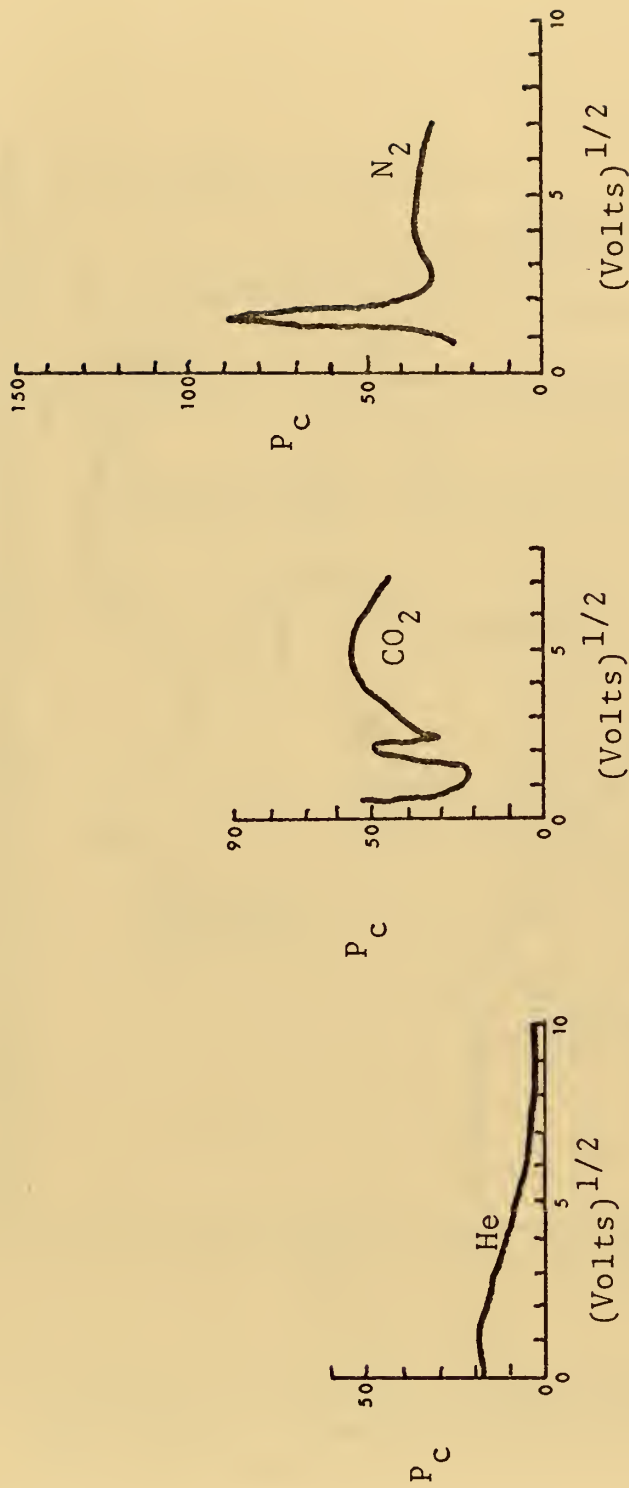
Electron Collision Probability

(Adapted from E. W. McDaniel, "Collision Phenomena in
Ionized Gases," John Wiley and Sons, Inc., New York, 1964)

FIGURE 10
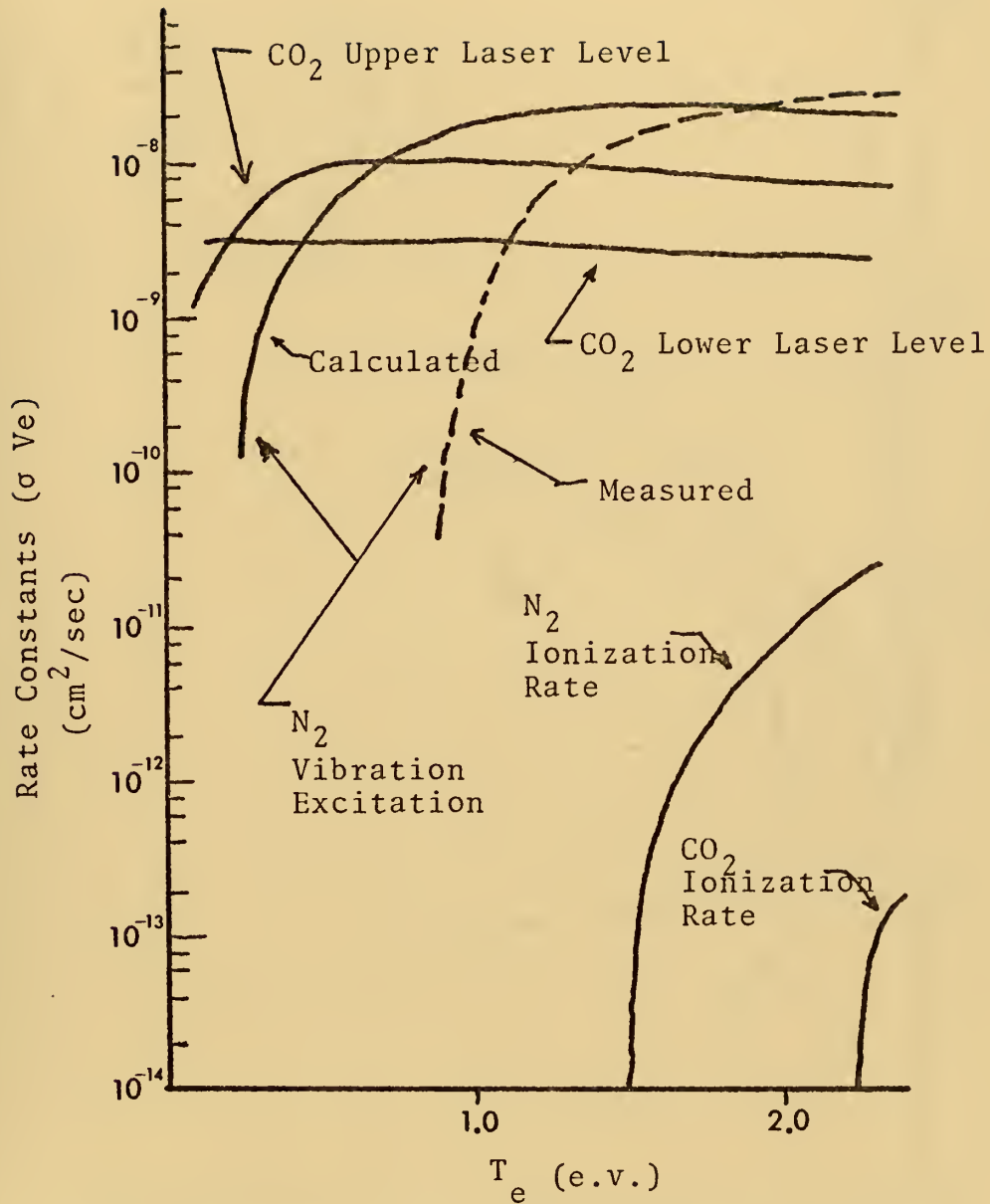
(Adapted from private correspondence with
AVCO Everett Research Laboratories, Everett,
Massachusetts, April 1972)

FIGURE 11
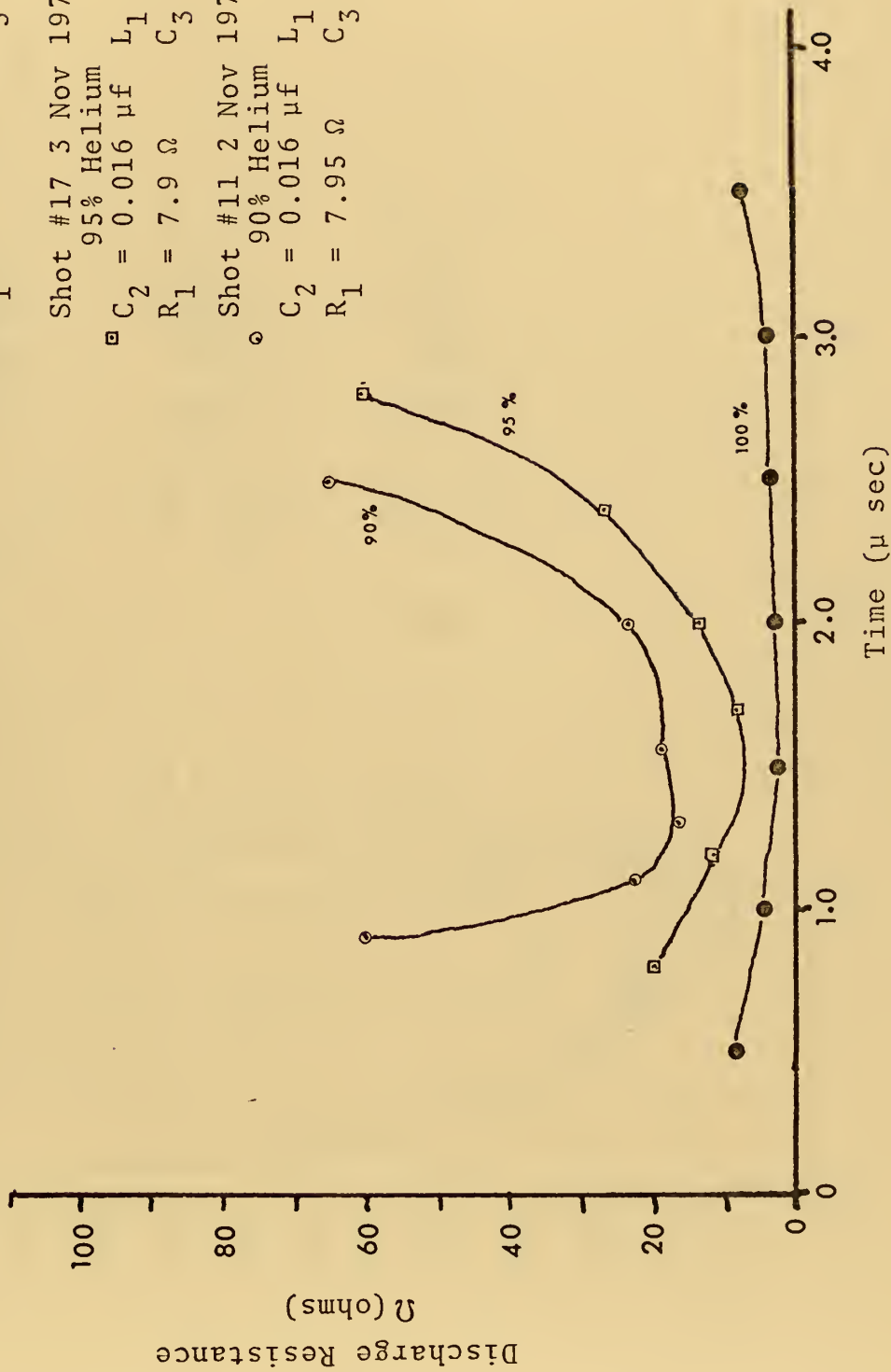
FIGURE 12

FIGURE 13

58
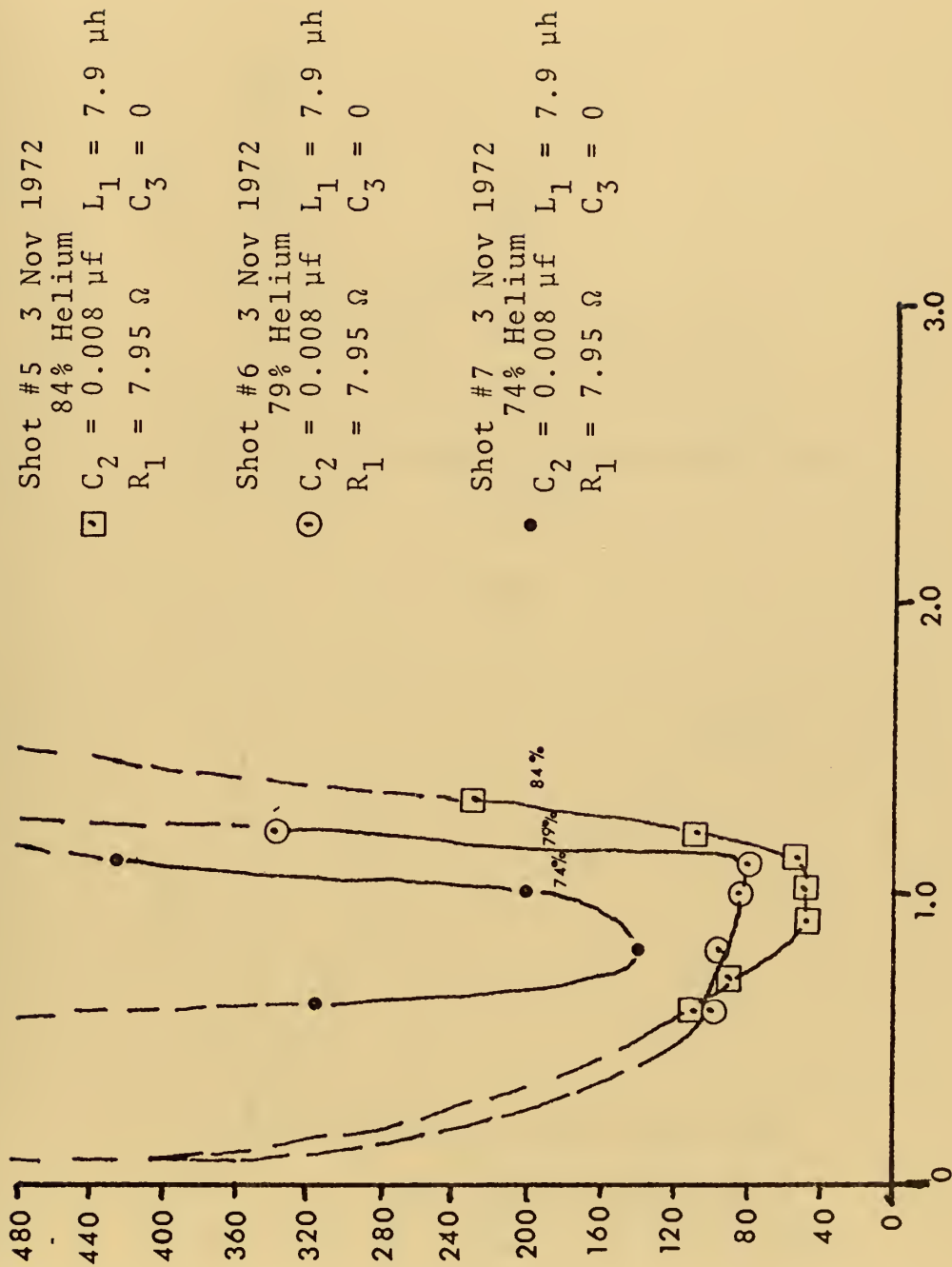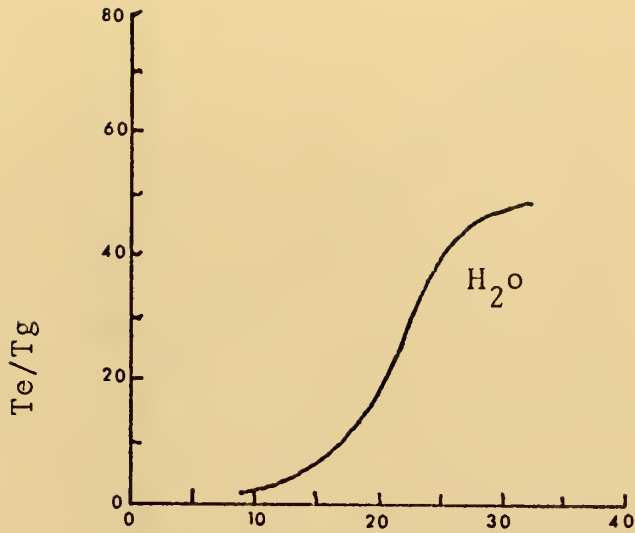
Ratio of Electron to Gas Temperature
in H_2O
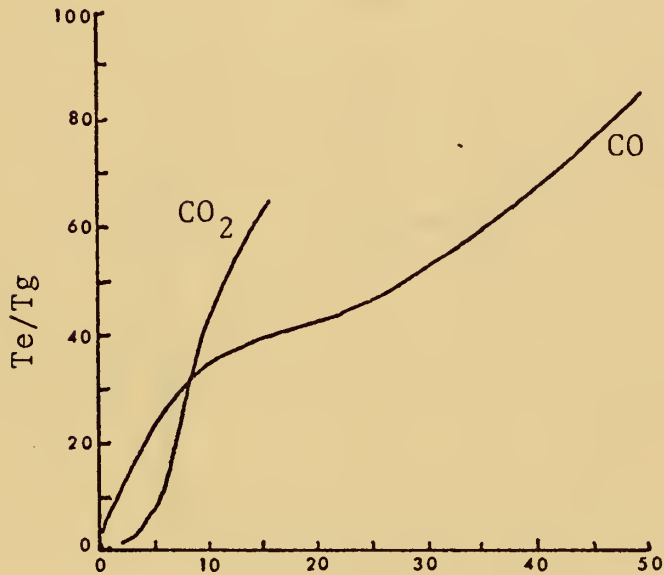
Ratio of Electron to Gas Temperature
in CO_2 and CO

(Adapted from S. C. Brown, "Basic Data of Plasma
Physics," John Wiley and Sons, Inc., New York, 1959)

FIGURE 14

E/p (Volts/cm/mm Hg)
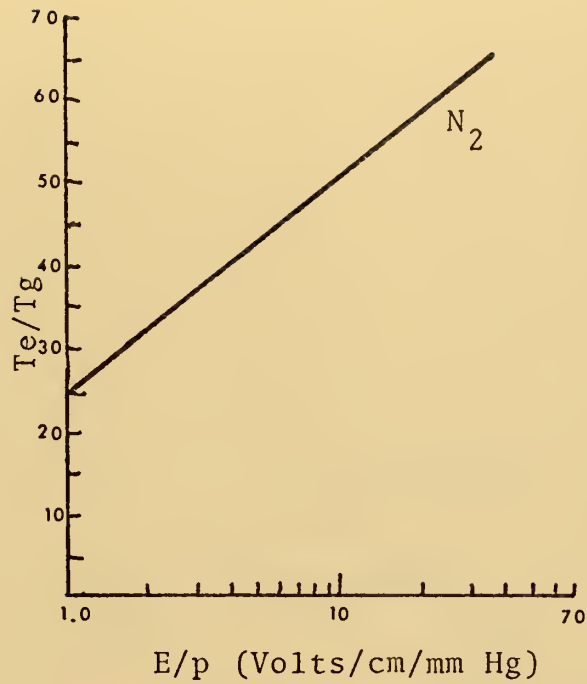
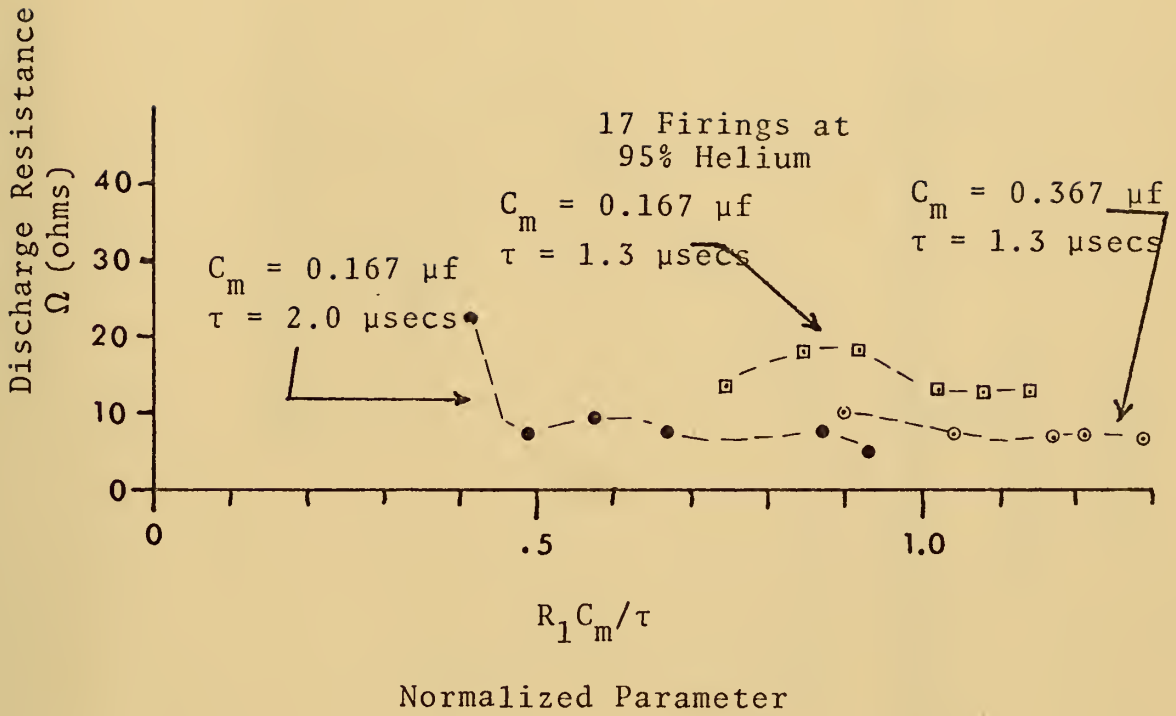Electron to Gas Temperature Ratio
for N_2

E/p (Volts/cm/mm Hg)
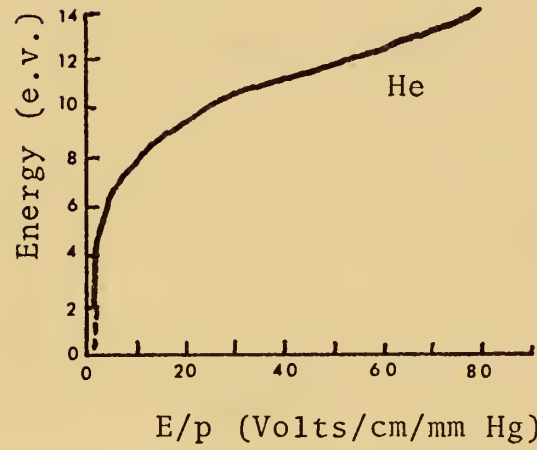
Average Energy of Electrons in
Helium

(Adapted from S. C. Brown, "Basic Data of Plasma
Physics," John Wiley and Sons, Inc., New York 1959)

FIGURE 15

FIGURE 16

61

Shot #19 3 Nov 1972
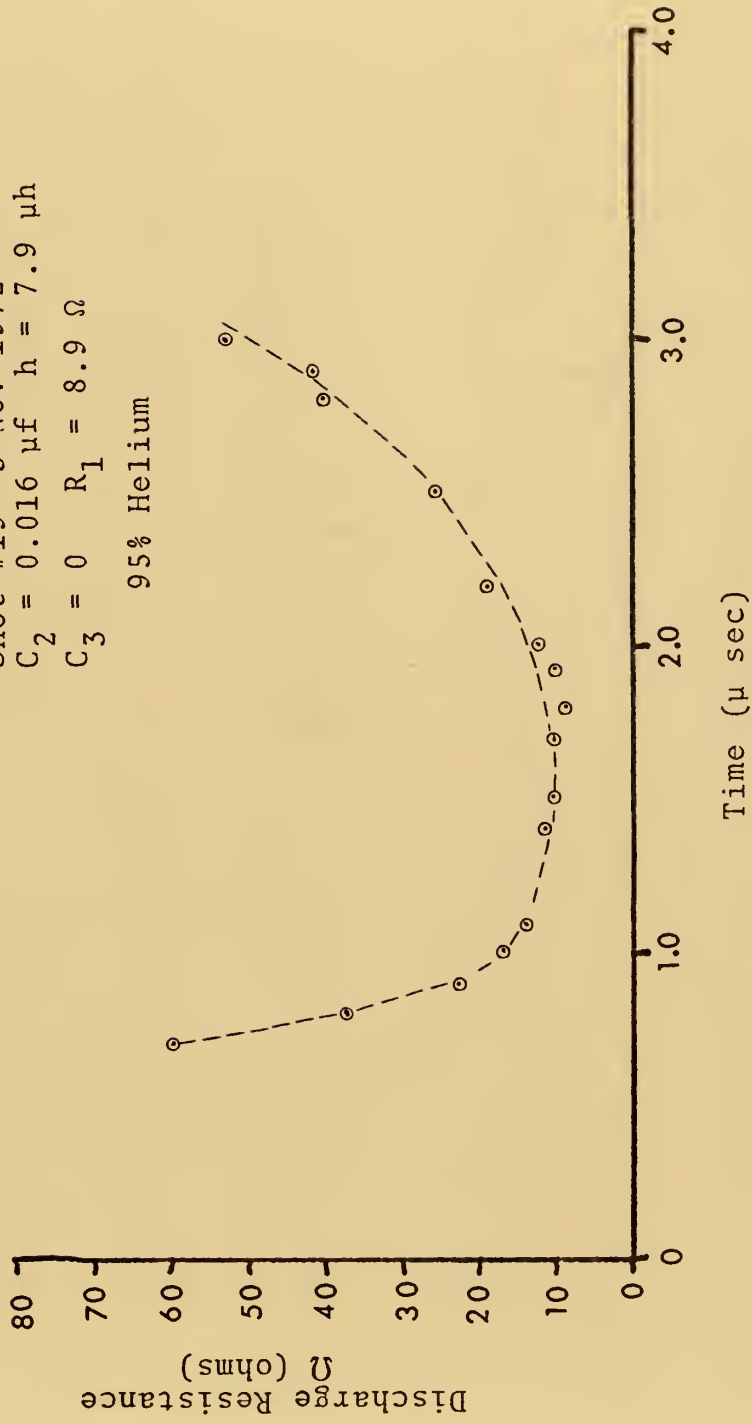$C_2 = 0.016$ μf h = 7.9 μh
$C_3 = 0$ $R_1 = 8.9$ Ω

95% Helium

Time (μ sec)

Discharge Resistance Ω (ohms)

FIGURE 17

Shot #7 8 Nov 1972
$C_2 = 0.016$ µf $C_3 = 0$
$L_1 = 11.5$ µh $R_1 = 4.76$ Ω
95% Helium

Arc Formation

Arc Maximum Intensity
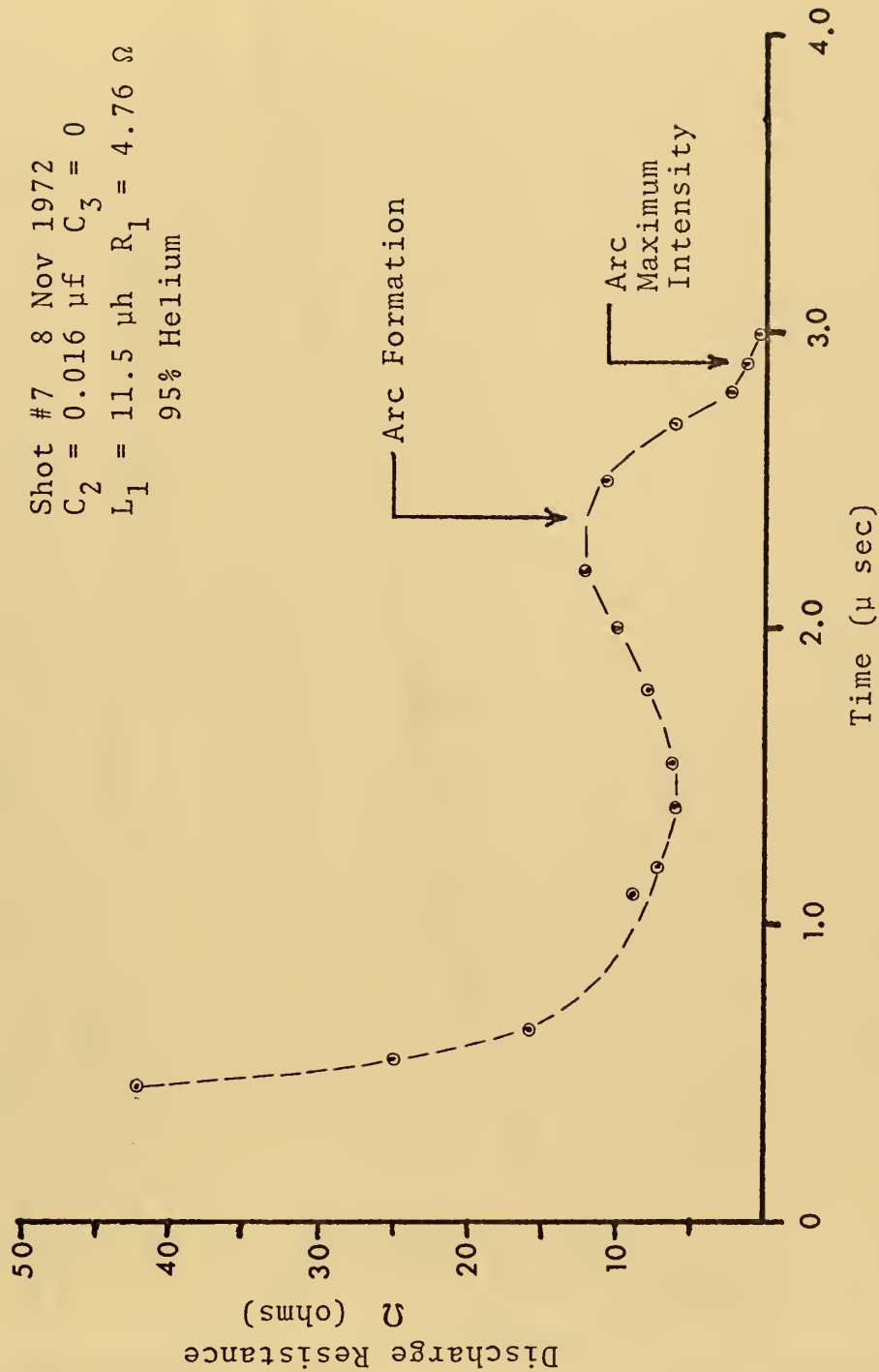
Time (µ sec)

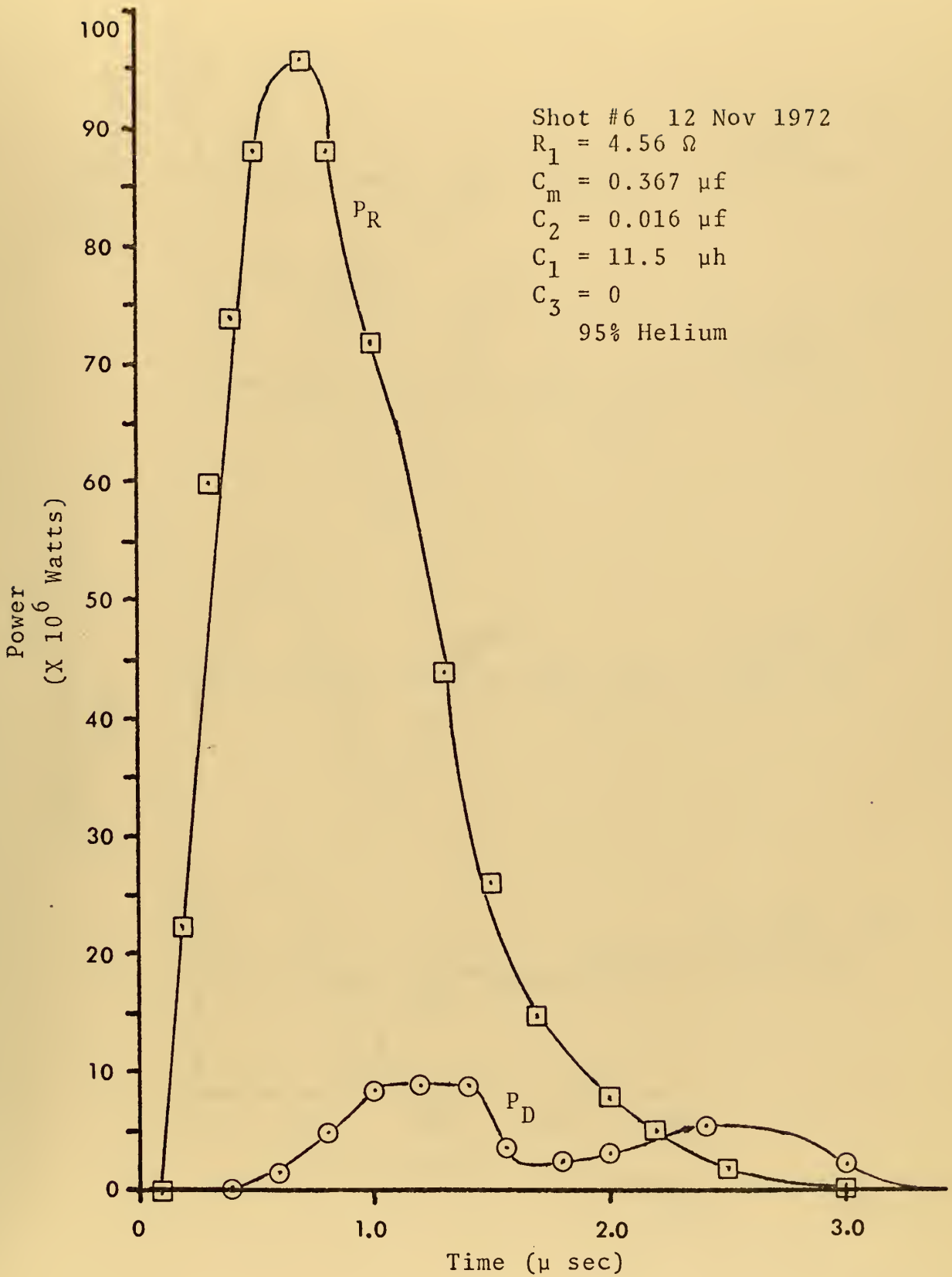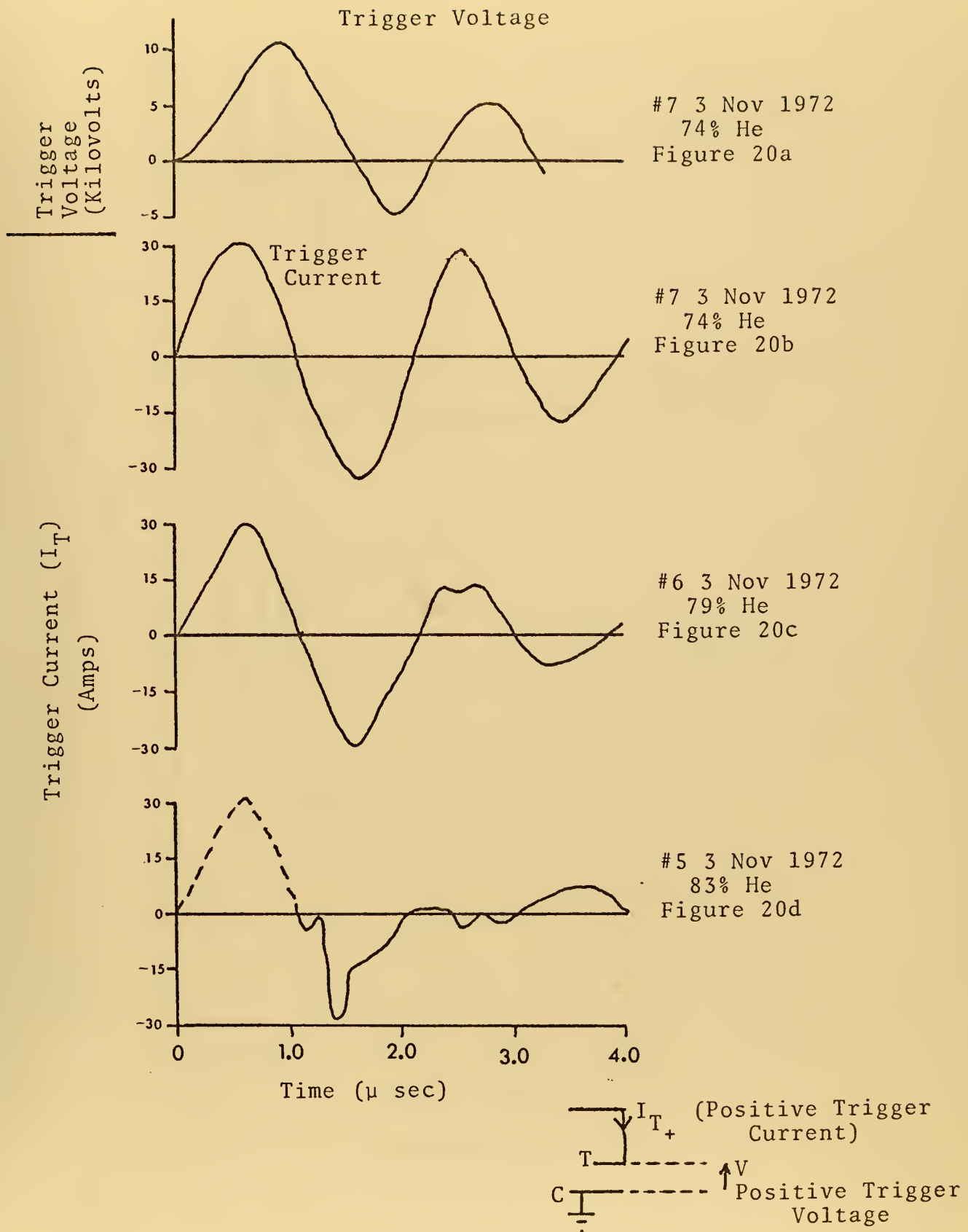Discharge Resistance Ω (ohms)

FIGURE 18

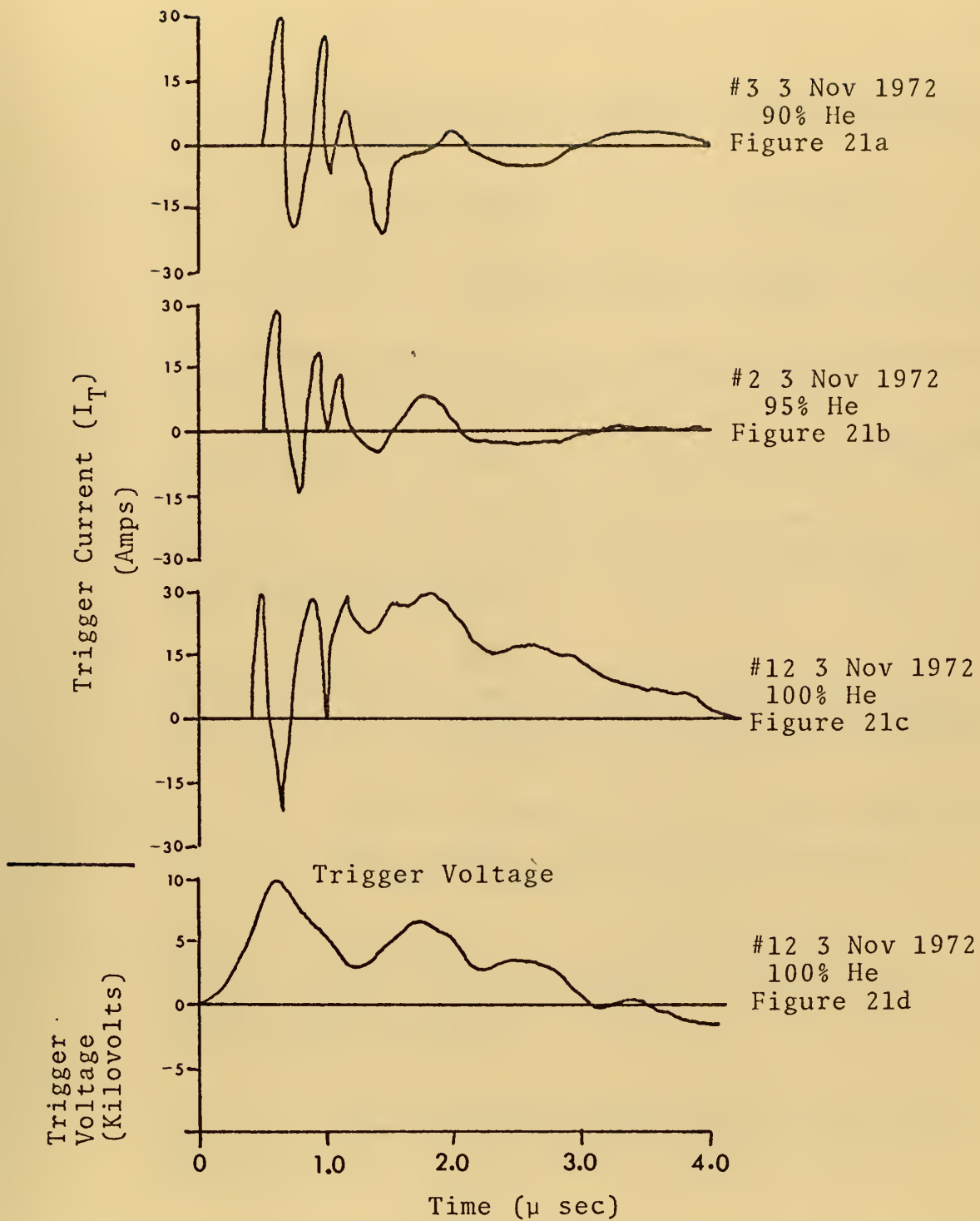FIGURE 19

64

FIGURE 20

65

FIGURE 21

LIST OF REFERENCES

1. Barr, D. H., <u>Construction of a Carbon Dioxide TEA Laser</u>, Master Thesis, Naval Postgraduate School, Monterey California 1972.

2. Pearson, P. R. and Lambertson, H. M., "Atmospheric Pressure CO_2 Lasers Giving High Output Energy Per Volume Unit," <u>IEEE Journal of Quantum Electronics</u>, V. QE-8, No. 2, p. 145-149, February 1972.

3. Ace Glass Incorporated, Vineland, New Jersey, Supplement Number 1, Ace Catalog Number 50, April 1961.

4. Beaulieu, J. A., "High Peak Power Gas Lasers," <u>Proceedings of the IEEE</u>, V. 59, No. 4, p. 667-674, April 1971.

5. LaFlamme, A. K., "Double Discharge Excitation for Atmospheric Pressure CO_2 Lasers," <u>The Review of Scientific Instruments</u>, V. 41, No. 11, p. 1578-1581, November 1972.

6. Pan, Y. L., Bernhardt, A. F., and Simpson, J. R., "Construction and Operation of a Double-Discharge TEA CO_2 Laser," <u>The Review of Scientific Instruments</u>, V. 43, No. 4, p. 662-666, April 1972.

7. Smith, D. C., "Thermal Defocusing of CO_2 Laser Radiation in Gases," <u>IEEE Journal of Quantum Electronics</u>, V. QE-5, No. 12, p. 600-606, December 1969.

8. McNice, G. T., and Derr, V. E., "Analysis of the Cylindrical Confocal Laser Resonator Having a Single Circular Coupling Aperture," <u>IEEE Journal of Quantum Electronics</u>, V. QE-5, No. 12, p. 569-575, December 1969.

9. Wolfe, W. L., <u>Handbook of Military Infrared Technology</u>, Office of Naval Research, Department of the Navy. Available from U.S. Government Printing Office, Washington, D.C., 1965.

10. T and M Research Products, Inc., <u>Current Viewing Resistor Catalog</u>, January 1972.

11. Judd, O., and Wada, J., "Plasma Conditioning by UV Preionization in a CO_2 Gas Laser," <u>Bulletin of American Physical Society</u>, V. 17, Series II, No. 11, p. 1054, November 1972.

12. Brown, S. C., *Basic Data of Plasma Physics*, p. 247-
     257, John Wiley and Sons, Inc., New York, 1959.

13. Private communication with Dr. Frank Chen, Professor
     of Physics, UCLA, November 1972.

14. Private communication with Dr. Yu-Li Pan, Lawrence
     Livermore Laboratories, Livermore, California,
     August 1972.

INITIAL DISTRIBUTION LIST

No Copies

1. Defense Documentation Center   2
   Cameron Station
   Alexandria, Virginia   22314

2. Library, Code 0212   2
   Naval Postgraduate School
   Monterey, California   93940

3. Assoc Professor Fred R. Schwirzke   2
   Code 61Sw
   Department of Physics and Chemistry
   Naval Postgraduate School
   Monterey, California   93940

4. Asst Professor Natale M. Ceglio   5
   Code 61C1 (Thesis Advisor)
   Department of Physics and Chemistry
   Naval Postgraduate School
   Monterey, California   93940

5. LT Ronald F. Bishop, USN   1
   7550 Comanche Drive
   Richmond, Virginia   23225

DOCUMENT CONTROL DATA - R & D

(Security classification of title, body of abstract and indexing annotation must be entered when the overall report is classified)

1. ORIGINATING ACTIVITY (Corporate author)	2a. REPORT SECURITY CLASSIFICATION
Naval Postgraduate School Monterey, California 93940	Unclassified
	2b. GROUP

3. REPORT TITLE

Discharge Characteristics of a Carbon Dioxide TEA Laser

4. DESCRIPTIVE NOTES *(Type of report and inclusive dates)*
Master's Thesis; December 1972

5. AUTHOR(S) *(First name, middle initial, last name)*

Ronald Floyd Bishop

6. REPORT DATE	7a. TOTAL NO. OF PAGES	7b. NO. OF REFS
December 1972	71	14

8a. CONTRACT OR GRANT NO.	9a. ORIGINATOR'S REPORT NUMBER(S)
b. PROJECT NO.	
c.	9b. OTHER REPORT NO(S) *(Any other numbers that may be assigned this report)*
d.	

10. DISTRIBUTION STATEMENT

Approved for public release; distribution unlimited.

11. SUPPLEMENTARY NOTES	12. SPONSORING MILITARY ACTIVITY
	Naval Postgraduate School Monterey, California 93940

13. ABSTRACT

During the past two years a rapid development in the field of high pressure CO_2 lasers has been witnessed. However, in the haste of this development very little effort had been expended to understand the detailed aspects of the discharge characteristics of such lasers. The results of a parametric study of the discharge characteristics of an atmospheric pressure, double-discharge CO_2 laser are reported. The results discussed include: A clarification of the important role played by helium in establishing good discharge conditions; measurements of plasma resistivity as a function of gas content and circuitry elements; establishment of a satisfactory operating regime in parameter space for a double-discharge laser with a two-centimeter gap; and a discussion of the major problems limiting the operation of such a laser. The results presented should be applicable to a wide class of double-discharge gas lasers.

DD FORM 1473 (PAGE 1)
1 NOV 65

S/N 0101-807-6811

A-31408

14. KEY WORDS	LINK A		LINK B		LINK C	
	ROLE	WT	ROLE	WT	ROLE	WT
TEA Laser						
Carbon Dioxide Laser						
Transverse Excitation						
Pulsed Power						
Infrared Radiation						
Marx Generator						
Double-Discharge Diagnostics						